Time Resolved Infrared Analysis of $AppA_{BLUF}$ using Isotopic Labeling at Mutant Studies

Contact s.meech@uea.ac.uk; ptonge@notes.cc.sunysb.edu

Allison Haigney
Stony Brook University
Dept of Chemistry, Stony Brook, NY 11794-3400, USA

Rui-Kun Zhao
University of East Anglia
School of Chemistry, Norwich, NR4 7TJ, UK

Peter J. Tonge
Stony Brook University
Dept of Chemistry, Stony Brook, NY 11794-3400, USA

Adelbert Bacher
Technische Universität München
Lehrstuhl für Organische Chemie and Biochemie, D-85747 Garching, Germany

Greg Greetham
Central Laser Facility
Harwell Science Facility, Didcot, Oxon OX11 0QX, UK

Ian Clark
Central Laser Facility
Harwell Science Facility, Didcot, Oxon OX11 0QX, UK

Werner Römisch-Margl
Technische Universität München
Lehrstuhl für Organische Chemie and Biochemie, D-85747 Garching, Germany

Andras Lukacs
University of East Anglia
School of Chemistry, Norwich, NR4 7TJ, UK

Richard Brust
Stony Brook University
Dept of Chemistry, Stony Brook, NY 11794-3400, USA

Stephen R. Meech
University of East Anglia
School of Chemistry, Norwich, NR4 7TJ, UK

Michael Towrie
Central Laser Facility
Harwell Science Facility, Didcot, Oxon OX11 0QX, UK

Introduction

Blue light using FAD (BLUF) domain proteins exist in many species with a variety of functions [1-5]. BLUF domain proteins bind flavin noncovalently in order to sense and respond to the intensity of blue (450 nm) light. AppA is the first and best characterized BLUF domain photoreceptor and is found in *Rhodobacter sphaeroides* where it acts as an antirepressor of photosystem biosynthesis. AppA consists of two domains: the N-terminal BLUF domain and a C-terminal domain that is responsible for the oxygen sensitivity of the protein. Our initial studies have focused on a truncated form of AppA that consists only of the N-terminal domain ($AppA_{BLUF}$). Initial studies of the BLUF domain identified early structural changes in photoactivity [1]. These studies determined the formation of a signaling state which is characterized by a 10 nm red shift in λ_{max} of the flavin chromophore. Currently, the goal is to understand the underlying chemical structures of the dark and signaling state of AppA by using spectroscopic analysis.

Isotope Labeling of the Flavin Chromophore

The normal chromophore in AppA is flavin adenine dinucleotide (FAD). Since isotope labeling of the isoalloxazine ring in FAD requires first synthesis of the ring and then biosynthetic conversion to FAD, which is a multistep process, we have initially concentrated our studies on the FAD analogue riboflavin (Rf, **Figure 1**). We reconstituted $AppA_{BLUF}$ with riboflavin (Rf) labeled with ^{13}C in the C2=O ([2-$^{13}C_1$]Rf) and C10a/C4=O ([4,10a-$^{13}C_2$]Rf) carbons of the isoalloxazine ring. Although we were successful in obtaining time resolved infrared (TRIR) spectra of the reconstituted protein, the low solubility of Rf has hindered preparation of the high concentrations of protein required for the spectroscopic studies. In addition, due to complexities in the vibrational data we have been very interested in labeling only the C4=O without introducing isotopes into other positions of the isoalloxazine ring. This has driven the synthesis of monoisotopomers of FAD. Importantly, we now have [2-$^{13}C_1$]FAD as well as FAD in which the oxygen in the C4=O isoalloxazine carbonyl has been replaced with ^{18}O ([4-$^{18}O_1$]FAD). This represents a major breakthrough give the number of steps involved in the synthesis of labelled FAD molecules.

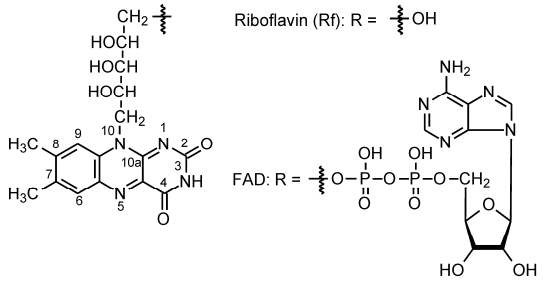

Figure 1: Structures of Riboflavin and FAD.

Currently we have obtained TRIR data of [2-$^{13}C_1$]FAD abound to $AppA_{BLUF}$ (**Figure 2**) and are in the process of collecting TRIR data on [4-$^{18}O_1$]FAD bound to $AppA_{BLUF}$. An important aspect of both the light and dark $AppA_{BLUF}$ [2-$^{13}C_1$]-FAD spectra is the appearance of an intense transient at 1660 cm^{-1} (**Figure 2**). This mode is seen in the unlabeled spectra at 1669 cm^{-1} in $dAppA_{BLUF}$.[6] It is unclear whether the 1660 cm^{-1} mode can be assigned to the C4=O excited state stretch, and it is plausible that this mode is delocalized among protein-chromophore interactions as opposed to being simply a flavin carbonyl stretch. The possibility that this transient reflects photoinduced modifications of flavin excited state - protein coupling will be tested by recording TRIR spectra of isotope edited AppA.

In addition we are performing a careful analysis of the effect of deuteration on the vibrational data of both chromophore and protein. By necessity most TRIR data on proteins are obtained using buffers dissolved in D_2O since this creates a 'window' in the IR spectrum between 1800 and 1400 cm^{-1}. However there are significant differences in the effect of

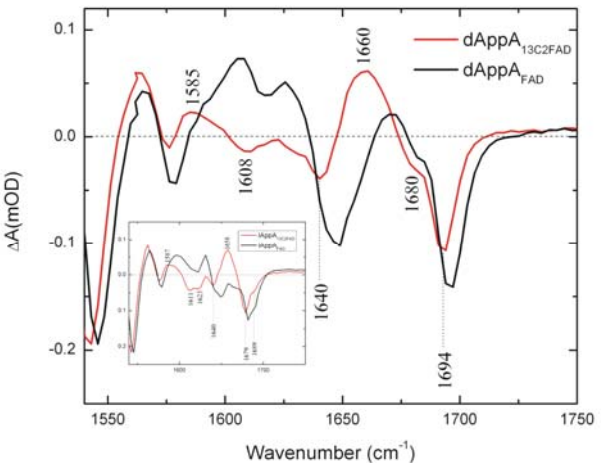

Figure 2: TRIR Spectra of $AppA_{BLUF}$ Bound to Unlabeled FAD and [2-$^{13}C_1$]FAD.

^{13}C labelling on the IR spectra of FAD in H_2O and D_2O. We have established that deuteration at N3 (N3-H to N3-D) alters the coupling between the C2=O and C4=O groups in the isoalloxazine ring. Since coupling is affected by deuteration, the effect of ^{13}C labelling will thus depend on whether spectra are collected in H_2O or D_2O. Our plans are to obtain TRIR data of $AppA_{BLUF}$ in H_2O buffer but this is a very challenging experiment since short path length cells must be used (6 μm instead of the normal 50 μm).

Isotope Labeling of the AppA Protein

The 1669 cm^{-1} transient observed in the TRIR spectrum of $dAppA_{BLUF}$ has been described previously as a photoactive marker and is only seen in $AppA_{BLUF}$ mutants that undergo a photocycle. This mode has previously been assigned to the amide side chain of Q63 which is thought to rotate or undergo keto-enol tautomerism upon photoexcitation. We have expended a very significant effort in attempts to isotopically label this glutamine in $AppA_{BLUF}$. This has included generating a variant of $AppA_{BLUF}$ (6Q-N) in which all the glutamines apart from Q63 (6) have been replaced with asparagines. Remarkably the 6Q-N $AppA_{BLUF}$ has a photocycle indistinguishable from the wild-type protein. However we have so far been unsuccessful at selectively labeling Q63 in 6Q-N $AppA_{BLUF}$. This has been attempted by growing cells expressing this protein on labeled glutamine and using a transaminase-deficient cell line to reduce scrambling of label. Currently, yields of protein are too low to permit the analysis required to ensure isotope incorporation.

While we attempt to improve the yield of the 6Q-N $AppA_{BLUF}$ protein, we have expressed the wild-type protein on minimal media containing $^{15}NH_4Cl$ so that all the nitrogens in the protein are labeled with ^{15}N. This approach will allow us to identify protein modes in the TRIR difference spectra. In particular, if the 1669 cm^{-1} transient is due to the Q63 amide side chain, then this mode should be sensitive to ^{15}N labeling. Uniformly labeled $AppA_{BLUF}$ will be studied during our next RAL trip.

Mutants of $AppA_{BLUF}$

We have generated the following $AppA_{BLUF}$ mutants: W104A, M106F, M106A, W104A/M106F, S41T, Q63E, Y21S and Y21C. These amino acids are distributed around the isoalloxazine ring (**Figure 3**) and all have been proposed to play key roles in the AppA photocycle. We will not describe in detail here all the results of each mutation, the Q63E $AppA_{BLUF}$ is extremely interesting. Previous models of AppA excitation incorporated changes in hydrogen bonding interactions involving Q63. Several mutants have been prepared of Q63, all

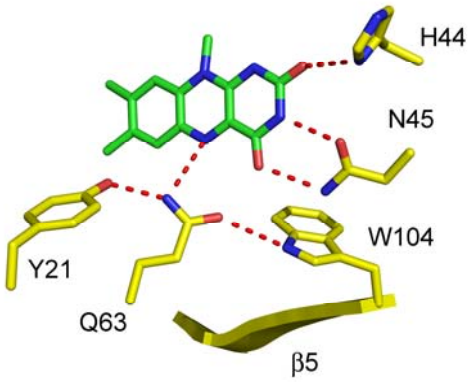

Figure 3: The Isoalloxazine Binding Pocket in AppA.

of which are photoinactive (such as Q63L) and that usually mimic the light adapted form of the protein. Q63E in contrast has spectroscopic properties that are intermediate between light and dark states. The TRIR spectra together with time resolved fluorescence and transient absorption measurements all indicate a unique protein-chromophore complex that, when fully characterized, should shed light on the structural changes that accompany photoactivation. Initial TRIR spectra are shown in **Figure 4** where it can be seen that major differences exist in the modes attributed to the flavin C=O groups. The 1650 cm^{-1} peak has split into two bands, while the highest wavenumber C4=O mode is shifted to 1720 cm^{-1}, consistent with reduced hydrogen bonding in the mutant. In addition, [4-$^{18}O_1$]FAD will be incorporated into this mutant to assign this mode the C4 carbonyl of FAD.

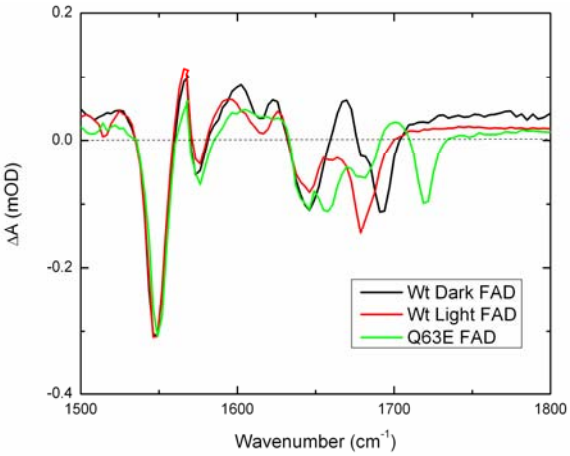

Figure 4: TRIR Spectra of Q63E $AppA_{BLUF}$
TRIR spectra (2mM, 3ps) are shown of $dAppA_{BLUF}$ (black), $lAppA_{BLUF}$ (red) and Q63E (green).

Conclusions

Both AppA's dark and light excited state dynamics have been studied using time resolved infrared spectroscopy (TRIR). TRIR spectra of unbound flavin were obtained and used to determine ground state and excited state modes. In addition, TRIR spectra of dark AppA and light AppA were also obtained and the differences between unbound flavin modes and those modes that correlated to protein or protein-flavin interactions were assigned. These studies showed some significant differences between the flavin, light and dark AppA [6].

We have used isotope labeling of both the flavin chromophore and of the protein in order to identify major differences in the TRIR spectra of light AppA and dark AppA. The data gathered allowed for the assignments of the C4 and C2 carbonyl modes that shift to lower frequency upon photoconversion to lAppA. In addition, we have studies

structurally conservative mutants of AppA using TRIR. These mutants, such as Q63E, shed light upon the sensitivity of the hydrogen bonding network of protein residues to the flavin.

Future work will include unnatural amino acid incorporation into position Y21 which has the potential to alter the kinetics of the photocycle by either eliminating or enabling electron transfer. Fluorotyrosines with a reduced pKa values compared to tyrosine have been introduced to Y21 and are thus expected to be valuable probes of the electron transfer reaction in which Y21 is thought to participate. TRIR measurements will give important information on how the kinetics are effected with the incorporation of various fluorinated tyrosines.

Acknowledgements

We are grateful to EPSRC (G002916) and NSF (CHE0822587) for financial support for this research and to STFC for facilities access.

References

1. Gomelsky, M. and G. Klug, *BLUF: a novel FAD-binding domain involved in sensory transduction in microorganisms.* Trends Biochem Sci, 2002. **27**(10): p. 497-500. 11. Iseki, M., et al., *A blue-light-activated adenylyl cyclase mediates photoavoidance in Euglena gracilis.* Nature, 2002. **415**(6875): p. 1047-51.

2. Okajima, K., et al., *Biochemical and functional characterization of BLUF-type flavin-binding proteins of two species of cyanobacteria.* J Biochem, 2005. **137**(6): p. 741-50.

3. Okajima, K., et al., *Fate determination of the flavin photoreceptions in the cyanobacterial blue light receptor TePixD (Tll0078).* J Mol Biol, 2006. **363**(1): p. 10-8.

4. Zirak, P., et al., *Photodynamics of the small BLUF protein BlrB from Rhodobacter sphaeroides.* J Photochem Photobiol B, 2006. **83**(3): p. 180-94.

5. Rajagopal, S., et al., *Purification and initial characterization of a putative blue light-regulated phosphodiesterase from Escherichia coli.* Photochem Photobiol, 2004. **80**(3): p. 542-7.

6. Stelling, A et al., *Ultrafast Structural Dynamics in BLUF Domains: Transient Infrared Spectroscopy of AppA and Its Mutants.* J. Am. Chem. Soc. 2008, **129**, p15556-15564.

High-resolution stimulated Raman spectroscopy with photoacoustic detection (PARS) of formic acid dimer

Contact Michael Hippler, *M.Hippler@sheffield.ac.uk*

Claire Louise Spencer, Christian Mohr and Michael Hippler

Department of Chemistry, University of Sheffield, Sheffield S3 7HF, England

Introduction

Spectroscopy is a powerful tool to probe intermolecular bonding. Raman and IR spectroscopy are complementary techniques, employing different selection rules. Quantum chemical calculations can be used in addition to spectroscopy to provide a deeper insight into bonding environments.

Hydrogen bonding X-H···Y, is an important intermolecular interaction. Usually a weakening of the X-H bond is involved, and hence a shift towards lower wavenumber ('red shift') of the XH-stretching vibration. Many recent works have shown evidence of a hydrogen bond which shows a strengthening of the X-H (*e.g.* C-H) bond and hence a shift towards higher wavenumber ('blue shift') in the XH-stretching vibration.

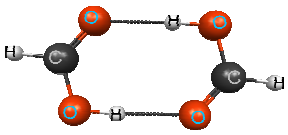

***Fig. 1**: CP-corrected MP2/6-311G(d,p)++ geometry of formic acid cyclic dimer.*

The lowest energy dimer conformation of formic acid (the cyclic dimer) has an energy low enough to be abundant and easily observable at room temperature in the gas phase. This cyclic dimer has predicted vibrational shifts towards lower (OH-stretching vibrations) and higher wavenumber (CH-stretching vibrations) and thus provides a unique opportunity to investigate the origin of vibrational shifts in more detail.

Raman spectroscopy can access the symmetric stretching vibrations, and infrared spectroscopy antisymmetric stretching vibrations. Conventional Raman experiments, however, suffer from low sensitivity and spectral resolution. More advanced techniques are therefore required to record Raman spectra of gas phase species with high sensitivity and sufficient spectral resolution.

High-resolution stimulated Raman spectroscopy with photoacoustic detection (PARS)

A stimulated Raman experiment with photoacoustic signal detection has been set up, which allows measuring Raman spectra of gaseous species with high resolution and sensitivity [1]. In the experiment, 532 nm laser light (second harmonic of a seeded Nd:YAG laser) is the Raman pump beam which is combined with the tuneable output around 630 nm of a dye laser as the stimulating beam and focused into a cell (EPSRC Laser Loan Pool, NSL1). If the energy difference between the laser photons corresponds to an allowed Raman transition, molecules are promoted to a vibrationally excited state by the stimulated Raman process. By collisions, the vibrational excitation is converted into local heating which creates a pressure wave which is picked up by a microphone (photoacoustic Raman spectroscopy, PARS, [1,2]). Since the seeded Nd:YAG laser has a very narrow bandwidth, the resolution of stimulated Raman scattering is only limited by the bandwidth of the stimulating dye laser (ca. 0.05 cm^{-1}).

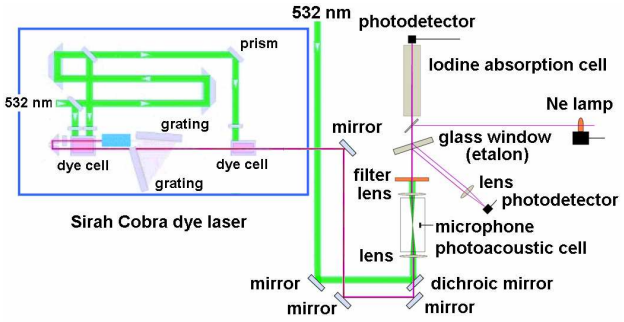

***Fig. 2**: Schematic of stimulated Raman photoacoustic setup.*

A system enabling accurate wavelength calibration of the tuneable dye laser has been set up and characterised, encompassing monitoring etalon fringes from a glass window, optogalvanic Ne spectroscopy, and monitoring iodine absorptions in a heated iodine vapour cell, achieving 0.03 cm^{-1} accuracy within a 20 nm scan range [1,3,4].

Extension of PARS to measure corrosive gases

The microphone inside the photoacoustic cell cannot sustain harsh environments like corrosive gas samples, as would be the case for measuring formic acid in the gas phase. We extended the PARS technique to the measurement of corrosive gases and hostile environments using a modification of the 'optophone' detection of Zare and coworkers [5]. In this approach, the pressure wave induced by light absorption distorts a membrane which has been gold coated to be corrosion resistant. The distortion is detected by a laser pointer and a split photodiode outside of the photoacoustic cell.

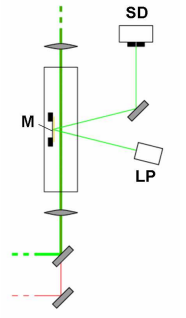

***Fig. 3**: 'Optophone' photoacoustic detection. M: gold-coated membrane; LP: laser pointer; SD: split photodiode.*

CH-stretching vibration of formic acid dimer

High-level quantum chemical calculations were performed to support the experiments, using the Gamess *ab initio* programme package with MP2 correction for electron correlations and the triple-zeta 6-311G(d,p)++ basis functions, and including a self-written program implementing Counterpoise Correction (CP) for the Basis Set Superposition Error (BSSE) [6]. The calculations predict a blue shift of 30 cm^{-1} for the Raman-active symmetric and 32 cm^{-1} for the IR-active antisymmetric CH stretching vibration upon dimerisation.

Stimulated Raman spectra have been acquired for gaseous formic acid, using the PARS technique described above with optophone detection of photacoustic signals. The CH-stretching vibration of both monomer and dimer formic acid has been observed (see fig. 4). The Raman-active symmetric CH-stretching vibration exhibits a shift towards higher wavenumber ('blue shift') of 7 cm^{-1} at room temperature.

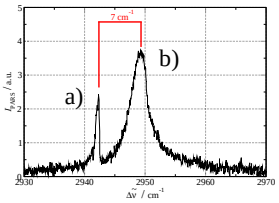

***Fig. 4**: Stimulated Raman photoacoustic spectrum (PARS) of formic acid (49 mbar) at room temperature.
(a) Monomer, (b) dimer.*

The IR-active antisymmetric stretching vibration has also been observed to investigate whether the vibrational shift can be partly attributed to the splitting between the symmetric and antisymmetric stretching vibration modes. FTIR spectra were obtained using a Perkin Elmer Spectrum 6X FTIR Serial 50895 machine, with a resolution of 0.2 cm^{-1}. Spectra obtained at high pressures (~20 mbar) will contain predominantly dimers, and at low pressures (~2 mbar) predominantly monomers. Suitable subtraction gives pure monomer and dimer spectra (see fig. 5).

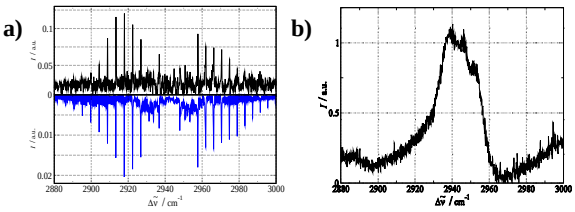

***Fig. 5:** (a) FTIR spectrum of gaseous formic acid monomer (~1.2 mbar) (top) and PGOPHER simulation (bottom).
(b) FTIR spectrum of gaseous formic acid dimer (~18.6 mbar).*

The monomer spectrum is well reproduced by a simulation using the PGOPHER programme [7]. IR spectroscopy shows a shift of ca. 4 cm^{-1} towards higher wavenumber ('blue shift') for the antisymmetric CH-stretching mode at room temperature.

The shift of the CH-stretching vibration towards higher wavenumber is thus genuine and not due to the splitting of the symmetric/antisymmetric modes. The shift is in qualitative agreement with the calculations, but smaller than calculated. This is most likely an effect due to thermal excitation; at room temperature, many low-frequency intermolecular vibrational modes are expected to be populated. This significantly weakens the hydrogen bond, and therefore the frequency shift induced by hydrogen bonding as a secondary effect is less pronounced. This effect shows clearly that theoretical calculations on weak hydrogen bonds which do not include thermal excitation can differ significantly from experimental observations at room temperatures (see also ref. [6]).

Mechanism of the vibrational frequency shift

Significant vibrational shifts are usually being associated with a bonding environment and have been used in the past as a signature of hydrogen bonding. The observed shift is thus unexpected and somewhat counter-intuitive at first, since the CH group is *not* involved in the hydrogen bonding of the cyclic dimer (see fig. 1). We propose that the shift is due to a secondary effect of the hydrogen bonding between the C=O and the O-H in cyclic formic acid dimer, based on our *ab initio* calculations.

The electric dipole moment of a bond is defined as partial charge multiplied by distance. If partial charges remain constant, then with increasing bond length, the dipole moment will increase. Our calculations show, however that for the C-H bond of formic acid the dipole moment will *decrease* with increasing bond length since partial charges of C and H are becoming weaker. This means that an increase in partial charges (polarity) in the C-H bond will lead to a compression and strengthening of the bond, causing a shift towards higher wavenumber ('blue shift') for the stretching vibration. The increase in polarity could be due to a secondary effect: upon formation of the hydrogen bond between O-H and C=O, the C=O bond becomes more polar which causes a withdrawing effect through the molecule, increasing the polarity and the strength of the CH group.

This mechanism will also apply for open dimer structures, and it will contribute significantly to the blue shift of the CH-stretching vibration predicted by *ab initio* calculations for these structures. The lowest energy open configuration of formic acid dimer, *e.g.*, has a strong OH···O bond, and a weaker CH···O hydrogen bond (see fig. 6).

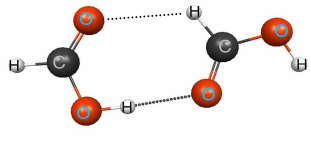

***Fig. 6**: CP corrected, MP2/ 6-311G(d,p)++ geometry of the lowest energy open configuration of acid dimer.*

Conclusions

Using a laser loan from the EPSRC Laser Loan Pool, we have successfully set up a stimulated laser Raman experiment with optophone photoacoustic detection which allows the observation of high-resolution Raman spectra of gas-phase species in hostile environments. With this technique, we have observed the CH-stretching vibration of formic acid dimer and found a distinct shift of this vibration towards higher wavenumber ('blue shift'). This shift is not directly due to intermolecular hydrogen bonding in the cyclic dimer. We propose that it is due to a secondary effect of the hydrogen bonding of the OH with C=O, where increase of electron density to the C=O bond by hydrogen bonding increases the polarity and strength of the C-H bond, thus inducing a shift towards higher wavenumber.

In future work, we would also like to apply this experimental technique to investigate the Raman-active symmetric OH-stretching vibration of cyclic formic acid dimer, for example to study the concerted double-proton transfer in the two equivalent OH···O hydrogen bonds in the nanosecond time domain.

Acknowledgements

A laser loan from the EPSRC Laser Loan Pool (NSL 1) is gratefully acknowledged. Our work is supported financially by the University of Sheffield.

References

1. M. Hippler and C. Mohr; Annual Report 2006/07, Central Laser Facilities, RAL, pg 120-123 (2007).
2. G.A. West, J.J. Barrett, D.R. Siebert, and K.V. Reddy, *Rev. Sci. Instrum.*, 1983, **54**, 797.
3. M. Hippler and J. Pfab, *Optics Comm.*, 1993, **97**, 347.
4. H. Salami and A.J. Ross, J. Mol. Spectr. **233**, 157 (2005).
5. M.-C. Chuang and R.N. Zare, *Chem. Phys. Lett.*, 1985, **115**, 47; S.M. Park and G.J. Diebold, *Rev. Sci. Instrum.*, 1987, **58**, 772.
6. M. Hippler, *J. Chem. Phys.*, 2005, **123**, 204311; M. Hippler, *J. Chem. Phys.*, 2007, **127**, 084306; M. Hippler, S. Hesse, and M.A. Suhm, "Quantum-chemical study and FTIR jet spectroscopy of $CHCl_3$ - NH_3 association in the gas phase", *Phys. Chem. Chem. Phys.*, in print, 2010.
7. PGOPHER, a Program for Simulating Rotational Structure, C. M. Western, University of Bristol, http://pgopher.chm.bris.ac.uk

Transient 2D-IR Spectroscopy of [FeFe]Hydrogenase Enzyme Model Compounds

Contact *nhunt@phys.strath.ac.uk*

A. I. Stewart, S.Santabarbara, S. Kaziannis, N.T. Hunt
Dept of Physics, University of Strathclyde
Glasgow, UK

J.A. Wright, C.J. Pickett
School of Chemical Sciences,
University of East Anglia, Norwich, UK

G. M. Greetham, M. Towrie, A.W. Parker
Central Laser Facility,
STFC Rutherford Appleton Laboratory

Introduction

The [FeFe]hydrogenases are a family of metalloenzymes with an active site based upon a 2Fe2S cluster in which the Fe atoms are coordinated by a mixture of carbonyl and cyano ligands. Interest in these systems is driven by the fact that they are capable of catalyzing the activation of molecular hydrogen. Furthermore, it has been shown that model compounds of the form (μSRS)Fe2(CO)6 are also capable of performing this function leading to the belief that these materials may form the basis for the next generation of catalytic materials for hydrogen fuel cells. [1-4]

In order to maximize the potential of these model systems in technological applications, it is imperative that we obtain a thorough understanding of their solution-phase chemistry and dynamics. One particularly relevant facet of their chemistry relates to the production of a vacant coordination site at one of the Fe centres. This is inherent in the active form of the enzyme and can be produced in solution by the photolytic removal of a carbonyl ligand.[5] Ultrafast infrared spectroscopy techniques have been shown to provide an effective probe of this process by virtue of the fact that carbonyl ligands give rise to structurally sensitive patterns of intense absorption bands in the spectrally uncongested region of the mid-IR at wavelengths near 5 μm. Recently, we have employed transient infrared pump-probe (TRIR) spectroscopy to study the carbonyl ligand photolysis of $(\mu S(CH_2)_3S)Fe_2(CO)_6$ [**1**] at 350 nm in heptane solution. This showed the formation of a complex set of photoproduct absorption bands consistent with CO ligand removal, but the linear nature of the data precluded definitive assignment of the peaks to a single photoproduct or mixture of species.[6] Ultrafast 2D-IR spectroscopy is a useful tool for problems such as this due to the ability to spread the molecular response over two frequency dimensions and thus give access to previously inaccessible information.[7,8] Applications of transient 2D-IR (T-2D-IR) spectroscopy to the photolysis of **1** in heptane have subsequently been used to determine both the vibrational coupling patterns of the photoproduct absorptions via the presence of off-diagonal peaks in the 2D spectrum and the relative appearance rates of these peaks following photolysis in order to assign the bands to a single photoproduct species.[9] Furthermore, these experiments observed a more rapid vibrational relaxation rate of the photoproduct in comparison to that of the parent,[10] allowing this single photoproduct to be assigned to a solvent adduct species in which the $Fe_2(CO)_5$ cluster was coordinated by a heptane molecule at the vacant site. Finally, it has been shown by ns-TRIR that photolysis of **1** in a mixed solvent consisting of a cyanoheptane in a molar majority of heptane leads to rapid formation of the heptane adduct from the first solvation shell followed by competitive substitution of heptane by the more strongly-coordinating solvent species. [11]

Here, we employ transient 2D-IR (T-2D-IR) spectroscopy to investigate the vibrational coupling patterns of the photolysis products of **1** in neat cyanoheptane in order to determine whether these too are consistent with the formation of a single solvent adduct photoproduct.

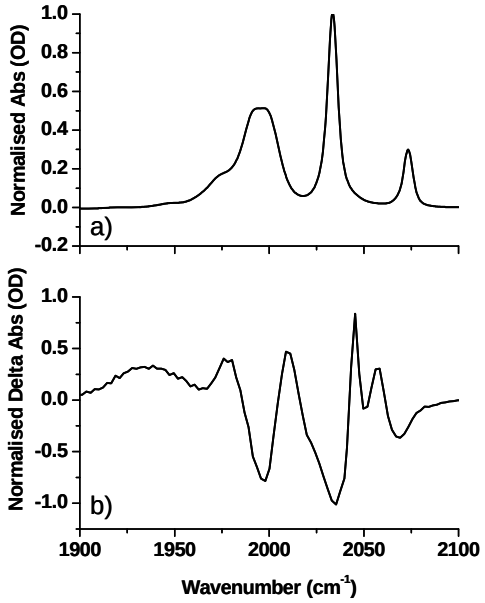

Figure 1: a) FTIR spectrum of ~1mM solution of 1 in cyanoheptane solution. b) TRIR spectrum of the same solution following phtoloysis at 350 nm. The data shown corresponds to a UV_{pump}-IR_{probe} delay time of 200 ps.

Experimental

The T-2D-IR spectrometer has been described in detail elsewhere.[12] Briefly, the ULTRA laser system was used to generate mid IR pump and probe pulses resonant with the CO stretching vibrations of **1** via optical parametric amplifiers (OPA) equipped with difference frequency mixing of the signal and idler beams. For 2D-IR spectroscopy, the narrow bandwidth (~10 cm^{-1}) pump pulse (IR_{pump}) was generated by an OPA pumped by the ps pulse duration arm of the twin synchronized regeneratively amplified Ti:sapphire laser systems, while the broad bandwidth (~400 cm^{-1}) IR_{probe} pulses originated from a second OPA pumped by the fs pulse duration regenerative amplifier. For T-2D-IR measurements, the UV photolysis pulse (UV_{pump}) was produced by a third OPA, pumped by the fs-regenerative amplifier and equipped with fourth harmonic generation capability in order to reach the required 350 nm wavelength.

The data presented here were recorded by modulating the amplitude of the two pump pulse trains (UV_{pump} and IR_{pump}) at one quarter and one half of the laser pulse repetition rate (10 kHz) respectively. This enabled TRIR, 2D-IR and T-2D-IR data

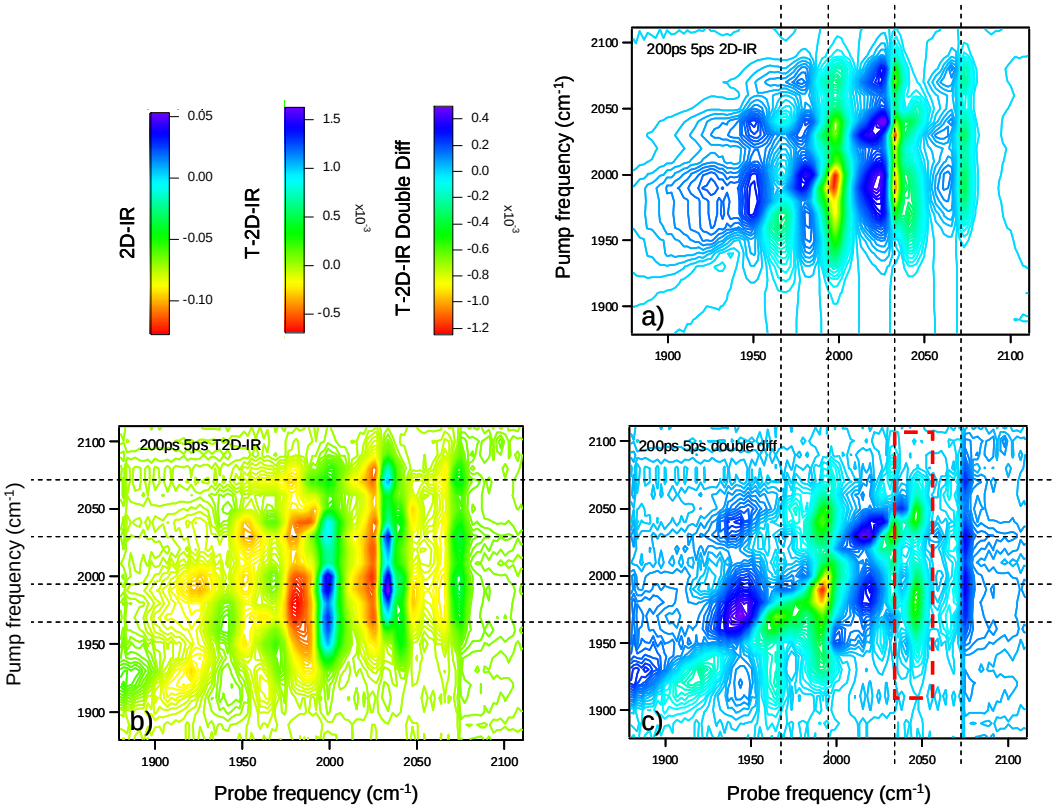

Figure 2: a) 2D-IR spectrum of 1 in cyanoheptane solution recorded with 5 ps IR_{pump}-IR_{probe} delay time and magic angle polarization relationship between IR_{pump} and IR_{probe} pulses. b) T-2D-IR data with 200 ps UV_{pump}-IR_{pump} delay time, 5 ps IR_{pump}-IR_{probe} delay time and parallel polarization relationship between UV_{pump} and IR_{probe} pulses and magic angle relationship between IR_{pump} and IR_{probe} pulses. c) Double difference T-2D-IR spectrum in which the data in a) has been scaled and subtracted from that in b) to reveal only peaks due to the photoproduct.

to be collected in sequential laser pulses along with a background signal (no pump pulses present).

The samples were held between CaF_2 windows separated by a PTFE spacer of 100 μm thickness. The solute **1** was produced and handled via established methods[1] and all solvents were obtained from Sigma Aldrich and used without further purification. To prevent sample degradation and window damage, the solution was flowed and the sample cell rastered in a plane perpendicular to the laser beam direction.

Results and Discussion

Figure 1 shows the FTIR spectrum and TRIR data for **1** in cyanoheptane solution. The FTIR spectrum (Fig 1(a)) consists of three intense transitions in the carbonyl stretching region, located at 2073, 2033 and 1997 cm^{-1}. These are very close to the absorption peaks observed for **1** in heptane solution,[10] though the significant broadening caused by the polar solvent leads to reduced spectral resolution to the point where it can only just be determined that the 1997 cm^{-1} peak consists of three overlapping transitions.

Upon photolysis at 350 nm with a UV_{pump}-IR_{probe} time delay of 200 ps, the TRIR spectrum of **1** (Fig 1(b)) shows three strong bleaches due to the loss of population of the parent molecules alongside positive features due to the formation either of hot parent molecules or photoproducts. The positive peaks are located at 2056, 2045, 2008, 1975 and 1930 cm^{-1} respectively though it is non-trivial to differentiate between them in terms of assignment via linear spectroscopy alone.

In order to assign these features more definitively, T-2D-IR spectra were obtained with a UV_{pump}-IR_{pump} time delay of 200 ps and an IR_{pump}-IR_{probe} time delay of 5 ps. The former was used to select a dynamically quiet region of the spectrum where the population of the photoproduct was, according to TRIR studies,[11] not changing dramatically, while the latter was chosen to maximize the signal strength of the T-2D-IR peaks and minimize coherence effects due to overlap between the IR_{pump} and IR_{probe} pulses. The results of these experiments are shown in Figure 2. Fig 2(a) shows the 2D-IR spectrum data channel, which should only show peaks due to the parent molecule. This is indeed the case, the negative peaks on the diagonal located at (ω_{probe}, ω_{pump}) = (2073, 2073), (2033, 2033) and (1997, 1997) correspond well to the v=0-1 transitions of the parent molecule while a peak located at (1975, 1975) is due to the shoulder observed in the FTIR spectrum at this frequency but which is better-resolved in the 2D-IR data by virtue of spreading the response over two axes. In each case, these diagonal features are accompanied by positive peaks shifted by 5-10 cm^{-1} to lower probe frequency that correspond to the v=1-2 transitions of the diagonal modes; the wavenumber shift is caused by the anharmonicity of the vibrational potential functions. Finally, each diagonal peak is linked to each of the other three by off-diagonal peak pairs that indicate vibrational coupling between the CO stretching modes. This is consistent with previous observations of the 2D-IR spectroscopy of **1** in organic solvents.[10]

These same features are present in the T-2D-IR channel (Fig 2(b)), though it is noted that he phase of these signals are reversed. By this, it is meant that the v=0-1 contributions become positive peaks while the red-shifted v=1-2 features are negative-going. This is caused by the presence of the UV_{pump} pulse in the T-2D-IR measurements leading to a reduced population of the parent molecule and a subsequent bleach of the 2D-IR peaks due to this species in the T-2D-IR spectrum. The difference-spectrum representation of the T-2D-IR spectrum means that these reversed phase features are the 2D equivalent of the bleaches observed in the TRIR data (Fig 1(b)).

Comparison of the T-2D-IR data with the 2D-IR channel also shows a significant number of additional features that are assignable to the 2D-IR spectrum of the photoproduct species. In particular these are located to lower pump and probe frequencies in the T-2D-IR data, consistent with the shift to lower frequencies observed for the CO stretching modes of **1** upon photolysis to form a pentacarbonyl species. This is attributable to the increased electron density back-donation to the remaining CO ligands. The broadening of the lineshapes caused by the cyanoheptane solvent leads to reduced resolution in the T-2D-IR data however and assignment of individual peak pairs is non-trivial. In order to accentuate the differences between the peaks due to the photoproduct and the parent molecule 2D bleaches, the 2D-IR spectral response (Fig 2(a)) was scaled and subtracted from the T-2D-IR data in Fig 2(b) to yield a double-difference spectrum (Fig 2(c)). The double difference spectrum thus contains only peaks due to the photoproducts, assuming a complete subtraction of the parent molecule peaks. In order to guide the eye, horizontal and vertical dashed lines from the 2D-IR and T-2D-IR spectra indicate parent molecule vibrational mode frequencies in Fig 2 so that the intersections of these lines on the double difference plot (Fig 2(c)) identify all of the parent molecule peak positions. Peaks not coinciding with these dashed guides are therefore assignable to photoproduct transitions.

The clearest region of the double difference spectrum where diagonal and off-diagonal photoproduct peaks are observed is highlighted by the red-dashed box. This corresponds to a vertical slice through the data at a probe frequency of 2050 cm^{-1}. This slice has been extracted and is shown in Fig 3. From fitting this slice to Gaussian lineshape functions, it is apparent that the diagonal peak is present at ~2045 cm^{-1} alongside a broad band centred at 1979 cm^{-1} and a third, smaller feature located at 1930 cm^{-1}. These indicate that the spectral response of the photoproduct peaks shows a diagonal peak near 2050 which is vibrationally coupled to modes near 1979 and 1930 cm^{-1}. In the case of the 1979 cm^{-1} transition, the increased width in comparison to the other two is suggestive of more than one overlapping transition as may be expected for a pentacarbonyl molecule lacking significant symmetry. It is noted that the combined effects of line broadening due to the solvent and the effects of convolution of the spectral lineshape with the pump pulse bandwidth profile significantly reduce the spectral resolution.

In the case of similar data recorded with heptane solution, photoproduct peaks were observed at 2050, 1999, 1978 and 1941. [9] Assuming that the broad peak is in fact two overlapping resonances and allowing for a solvatochromic shift attributable both the polar solvent and a more strongly coordinating species it is reasonable to assign the above set of transitions to a photoproduct species. Comparison of these peaks with those observed in Fig 1(b) therefore indicate that the transitions observed at 2056 and 2008 cm^{-1} are likely to be due to vibrational cooling as they show no coupling to the other photoproduct transitions. This is also consistent with their positions slightly to the red of the main photoproduct bleaches, implying that they belong to hot ground state species.

Conclusions

T-2D-IR spectroscopy has been employed to determine the infrared absorption frequencies and coupling patterns of the photoproduct vibrational modes of the species formed following photolysis of **1** in cyanoheptane. Double difference T-2D-IR analysis has revealed a number of peaks due to the photoproduct and they show spectroscopy consistent with the formation of a pentacarbonyl solvent adduct species. In the data presented here line broadening effects limit the ability to resolve all photoproduct diagonal and off-diagonal peaks, however the similarities between this data and that obtained in heptane are sufficient for a conclusion to be reached. Future studies using photon echo-derived 2D-IR methods under development will provide the improved spectral resolution required for observation of all the individual 2D peaks.

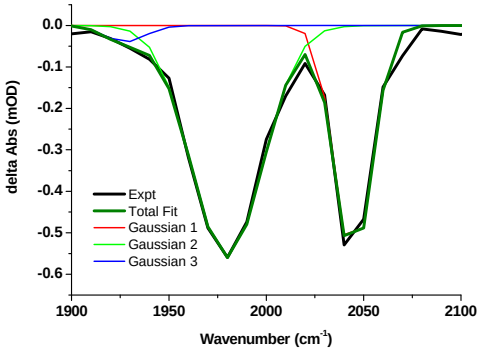

Figure 3: Slice through the T-2D-IR double difference spectrum in Fig 2(c) at a probe frequency of 2050 cm^{-1}. Thin lines show the results of fitting to three Gaussian lineshape functions.

Acknowledgements

The authors acknowledge funding from the EPSRC (NTH, AIS) and the European Research Council (NTH, SS, SK) as well as the BBSRC (JAW, CJP). The award of a STFC Programme Access grant is also acknowledged.

References

(1) Liu, X. M.; Ibrahim, S. K.; Tard, C.; Pickett, C. J. *Coordination Chemistry Reviews* **2005**, *249*, 1641.
(2) Borg, S. J.; Tye, J. W.; Hall, M. B.; Best, S. P. *Inorg Chem* **2007**, *46*, 384.
(3) Borg, S. J.; Behrsing, T.; Best, S. P.; Razavet, M.; Liu, X.; Pickett, C. J. *J Am Chem Soc* **2004**, *126*, 16988.
(4) Tard, C.; Liu, X. M.; Ibrahim, S. K.; Bruschi, M.; De Gioia, L.; Davies, S. C.; Yang, X.; Wang, L. S.; Sawers, G.; Pickett, C. J. *Nature* **2005**, *433*, 610.
(5) Silaghi-Dumitrescu, I.; Bitterwolf, T. E.; King, R. B. *J Am Chem Soc* **2006**, *128*, 5342.
(6) Ridley, A. R.; Stewart, A. I.; Adamczyk, K.; Ghosh, H. N.; Kerkeni, B.; Guo, Z. X.; Nibbering, E. T. J.; Pickett, C. J.; Hunt, N. T. *Inorg Chem* **2008**, *47*, 7453.
(7) Hunt, N. T. *Chem Soc Rev* **2009**, *38*, 1837.
(8) Hochstrasser, R. M. *Proc Nat Acad Sci* **2007**, *104*, 14190.
(9) Stewart, A. I.; Wright, J. A.; Greetham, G. M.; Kaziannis, S.; Santabarbara, S.; Towrie, M.; Parker, A. W.; Pickett, C. J.; Hunt, N. T. *Inorg Chem* **2010**, *(submitted)*.
(10) Stewart, A. I.; Clark, I. P.; Towrie, M.; Ibrahim, S.; Parker, A. W.; Pickett, C. J.; Hunt, N. T. *J Phys Chem B* **2008**, *112*, 10023.
(11) Kaziannis, S.; Santabarbara, S.; Wright, J. A.; Greetham, G. M.; Towrie, M.; Parker, A. W.; Pickett, C. J.; Hunt, N. T. *J Phys Chem B* **2010**, *submitted*.
(12) Kania, R.; Stewart, A. I.; Clark, I. P.; Greetham, G. M.; Parker, A. W.; Towrie, M.; Hunt, N. T. *PhysChemChemPhys* **2010**, *12*, 1051.

Ultrafast TRIR Studies on Tetraazidosilicon Complexes

P Portius,* J A Weinstein, M Davis, I V Sazanovich

Department of Chemistry, University of Sheffield, Sheffield, S3 7HF, UK

M Towrie, I P Clark

Central Laser Facility, CCLRC Rutherford Appleton Laboratory, Chilton, Didcot, Oxon, OX11 0QX, UK

Main contact email address: p.portius@sheffield.ac.uk

Introduction

Finding compounds that can both reliably store and release energy in a controlled manner is a great challenge. Nitrogen-rich compounds are often highly endothermic and, as high-energy density materials (HEDMs), store a lot of chemical energy.[1-3] Nitrogen-rich HEDMs have several superior properties over conventional explosives, propellants and pyrotechnics, mainly due to the fact that they release less smoke, toxic byproducts and green house gases.[4] Their main product of decomposition is dinitrogen. There are several ways to trigger energy release – reactions with light being one of them. Nitrogen-rich molecules, however, constitute a photochemically not well-investigated area.

Recently, we have prepared hexacoordinate tetraazido silicon complexes [3] (**1**-**3**, Scheme 1) as a new type of nitrogen-rich compounds. These complexes contain diimine ligands as chromophores and azido ligands. They are less friction sensitive, moderately air sensitive, colourless solids, which are soluble in a number of aprotic solvents. The azido ligands act as reporter groups and make these compounds ideal for mechanistic photochemical studies using time-resolved infrared (TRIR) spectroscopy.

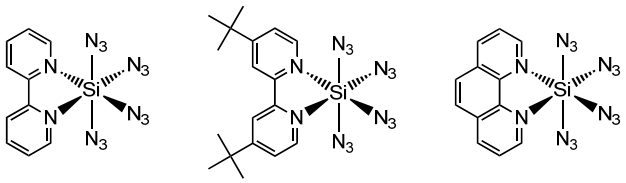

Scheme 1.

Preliminary results of picosecond (ps) and nanosecond (ns) TRIR experiments with solutions of $Si(N_3)_4$(bpy) (**1**), $Si(N_3)_4$($^tBu_2$bpy) (**2**) and $Si(N_3)_4$(phen) (**3**) are presented here as part of our ongoing EPSRC funded research program *Real-time structural dynamics of molecular systems for energy generation and storage*.[5]

Experimental arrangements

The complexes **1**-**3** were synthesized in adaptation of published procedures.[3] The PIRATE[6] and ULTRA[7] spectrometers were used for the ps- and ns-TRIR measurements. Solutions were prepared n dry degassed solvents, saturated with nitrogen and kept under slight pressure in a recirculating flow system at r.t. The optical density in the photolysis cells at λ_{exc} = 266 nm was kept below unity.

TRIR spectroscopy

TRIR spectra of the complexes **1**-**3** were obtained in acetonitrile (MeCN), tetrahydrofuran (THF) and CH_2Cl_2 solutions under 266 nm excitation, and registered in the region between 1920 cm^{-1} and 2260 cm^{-1}. In the following, the temporal evolution of the TRIR spectra of complex **1** (Scheme 1) is described in more detail.

The IR spectra of the largely C_2 symmetric tetraazido complexes **1**-**3** feature generally three intense bands in the mid infrared region which arise from four 'asymmetric' azide N-N-N vibrations of the symmetry species *A* and *B*. In THF solutions of complex **1** the parent bands at 2212, 2125 (shoulder) and 2149 cm^{-1} are fully bleached 4 ps after laser flash (266 nm) and several broad transient bands are present. These transients are centred at 1992 cm^{-1} (species X) and overlapped with the parent bleaches with apparent maxima at 2089 and 2138 cm^{-1} (Y) and 2161 cm^{-1} (Z) (Fig. 1, left).

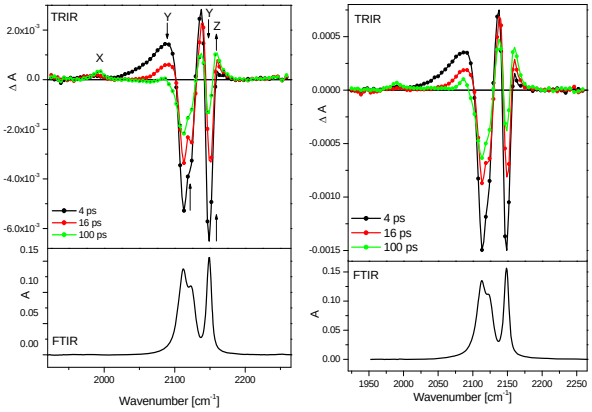

Figure 1. TRIR spectra in THF solution (λ = 266 nm, top row) at *t* = 4, 16 and 100 ps of $Si(N_3)_4$(bpy) (**1**, left) and $Si(N_3)_4$(phen) (**3**, right) and respective ground state FTIR spectra (bottom row).

Over the next 100 ps the bands associated with the transient Y (at 2089 and 2138 cm^{-1}) narrow and decay very fast, with the parent bleach bands recovering synchronously. The band narrowing and a hypsochromic of the single band of species X can also be discerned. A kinetic analysis of the decay of Y and the recovery of the parent estimated the lifetime for this process to values between 8 and 18 ps. Furthermore, the rise of an initially small transient band at 2162 cm^{-1} (Z) occurs during the decay of the transient Y (Fig. 2, red trace).

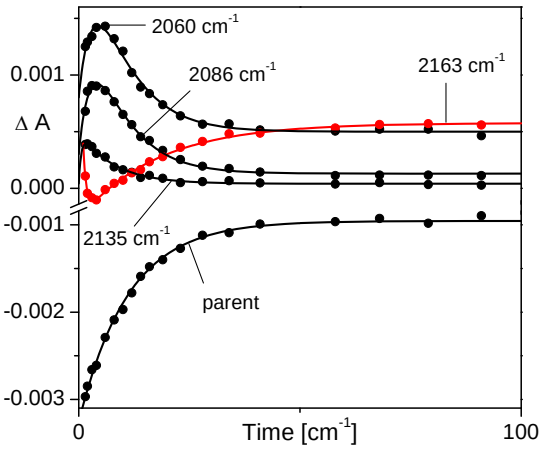

Figure 2. Kinetic traces of **1** in THF solution between 1 ps and 100 ps showing the decay of transients Y (black), the rise of transient Z (red) and partial recovery of a parent band.

In order to obtain more accurate spectral information the parent bleach bands were subtracted from the ps-TRIR spectra and the residual fitted using Voigt profiles (Fig. 3, left). For the TRIR spectrum at 100 ps this treatment afforded accurate peak maxima and approximate line widths for four transient bands at 1992 cm^{-1} (X), 2106, 2133 and 2156 cm^{-1} (Z). The bands associated with transient species Z persist throughout the investigated time delays up to 5000 ns. The single band of X can be assigned easily to the uncoordinated N_3 ligand or azide anion N_3^- , by comparison with FTIR spectra of THF solutions of salts containing this anion (e.g. $N(PPh_3)_2^+N_3^-$, 1993 cm^{-1}). The remaining bands (Z) arise from species with coordinated azido groups. See Table 1 for an overview of band positions.

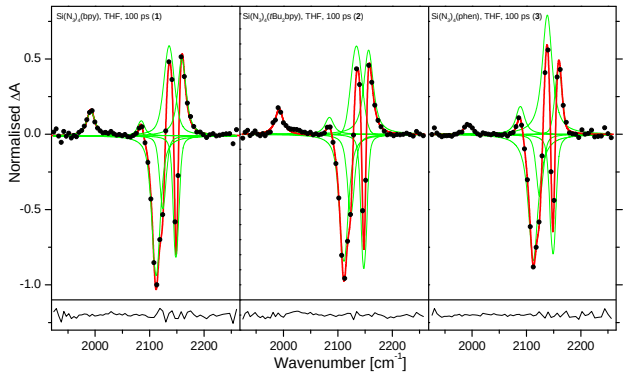

Figure 3. Difference TRIR spectra in THF solution (λ = 266 nm, top row) at *t* = 100 ps of compounds **1** (left), **2** (middle) and **3** (right). Spectra are normalised to the total area of the bleached parent absorptions; spectral points (black), Voigt profiles (green), fit curve (red), fit residues (bottom row).

The potential presence of anionic products prompted an investigation of the effect of polarity and coordination ability of the solvent. Studies performed in THF and CH_3CN revealed only minor differences in the position and temporal evolution of the transient bands observed in solutions of **1** in THF and MeCN on the 1 ps to 100 ps time scale (Fig. 4, Table 1). However, the ratio of band areas (N_3^- : transient) changes significantly from 1 : 7 in THF to 1 : 3 in MeCN. Hence, the stronger coordinating and more polar solvent (MeCN) promotes the formation of ionic photoproducts. The diimine ligand too has a marked, though less well understood, influence on the ratio of photoproducts. The 100-ps TRIR spectra in THF show a significantly enhanced formation of N_3^- for (4,4' disubstituted) bpy over phen complexes as shown by the ratios of band areas, 1 : 7 (bpy), 1 : 7 ($^tBu_2$bpy), 1 : 27 (phen).

In THF the N_3^- transient band (X) vanishes with a lifetime of 633±55 ns which is matched by the synchronous recovery of the parent bands. Parent recovery during this period amounts to only 40% of the total bleach and a close investigation of the features of the transients at 2106, 2133 and 2156 cm^{-1} reveals more subtle changes. These changes could be accounted for by expanding the model of Voigt profiles by two additional, less intense transients (Z') (see Table 1), which in the TRIR spectrum remain hidden throughout the observed times delays. A global curve fit using the expanded model reveals that the bands of Z remain unchanged while those of Z' decay completely. A kinetic analysis of the associated band area changes reveals that both parent recovery and the decay of the bands of X and Z' are synchronous on this time scale (Fig. 5).

A tentative mechanism can be drawn up at this stage (Scheme 2). Upon excitation of complex **1** an excited state is formed (transient Y), which fully decays within the first 50 ps. The decay leads in part to the reformation of the parent complex. The remainder is involved in photodissociation and reacts upon breaking a Si-N_α bond and formation of the azide anion (transient X) and a corresponding cationic silicon complex (transient Z') (*i*), and also upon breaking a N_α-N_β bond within one azido ligand generating dinitrogen gas and a nitrene complex (transient Z) (*ii*). N_α denotes the ligating N atom of the azido ligand. Recombination of the ionic products makes process (*i*) fully reversible. Reattachment of dinitrogen, however, is thermodynamically strongly disfavoured and hence process (*ii*) is irreversible. The presence of three long-lived transient bands (Z) points to a complex bearing three azido ligands. Preliminary results of DFT calculations (Dr. A. Meijer) indicate that a nitrene complex (as postulated in Scheme 2) is not a minimum on the energy hypersurface. Once the N_α-N_β bond is broken, the resultant 'nitrene' inserts into an adjacent Si-N bond.

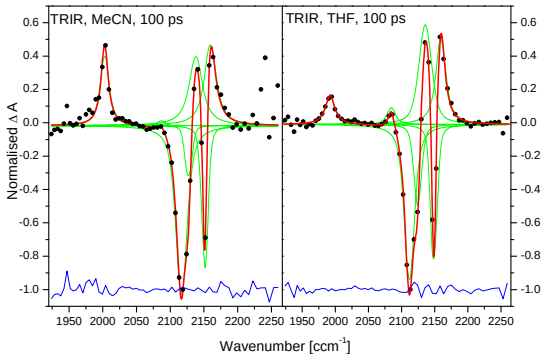

Figure 4. Difference TRIR spectra in THF solution (λ = 266 nm) at *t* = 100 ps of **1** ($Si(N_3)_4$(bpy)) in MeCN (left) and THF (right). Spectral points (black), Voigt profiles (green), fit curve (red), fit residues (blue lines).

Inspection of the combined ns- and ps-TRIR spectra of the related complexes **2** and **3** suggests that analogous mechanisms operate in the photoreactions of the latter.

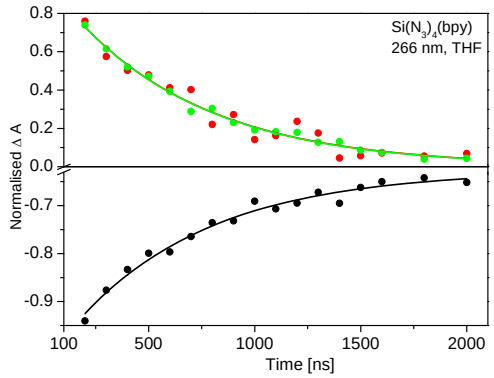

Figure 5. Kinetic traces of normalized band areas in a THF solution of from 200 ns to 2000 ns showing the synchronous decay of the transient bands of X (green) and Z' (red) and the recovery of the parent complex (black).

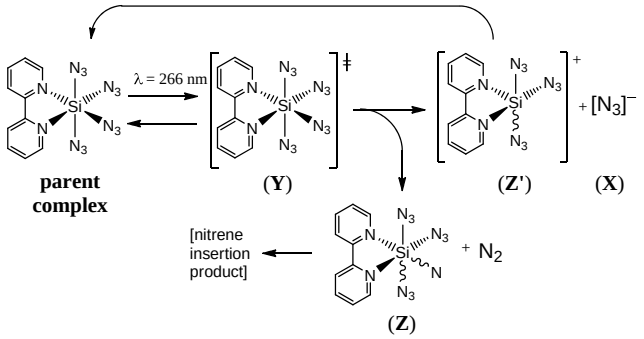

Scheme 2. Proposed reaction mechanism.

Conclusions

The photochemical behaviour of several new tetrazido silicon complexes has been investigated with the aim to identify a mechanism for photochemical energy release and the generation of dinitrogen. The precise nature of several transients is still unknown. Using the transient absorption capabilities of the ultrafast laboratory at the CLF we plan to further investigate the possibility of an electronic excited state being formed initially prior to breaking either Si-N_α or N_α-N_β bonds. Quantum chemical calculation performed in Sheffield (Dr. A. Meijer) on the minimum structures of the candidate species (Scheme 2) will provide frequencies for the asymmetric N-N-N stretch vibrations, which will then be used to match with the bands found in the TRIR experiments. The presented study has shown that using ps and ns TRIR spectroscopy is suited to unravel the mechanism of photochemically induced reaction in nitrogen-rich compounds.

Table 1. Band position [cm^{-1}] of ground states and transients determined from time resolved infrared spectra at ca. 30 ps (λ_{exc} = 400 nm) using pseudo Voigt profiles.

$Si(N_3)_4L$ L =	Parent Bands	Transient Bands
Solvent: CH_3CN		
bpy	2116, 2127, 2151	2002 (X) 2087, 2138, 2159 (Z)
$^tBu_2$bpy	2115, 2125, 2150	
phen	2116, 2126, 2150	2005 (X) 2092, 2135, 2158 (Z)
Solvent: CH_2Cl_2		
bpy	2115, 2127, 2152	-
phen	2116, 2127, 2152	-
Solvent: THF		
bpy	2212, 2125, 2149	1992 (X) 2106, 2133, 2156 (Z) (2121, 2156) (Z')
$^tBu_2$bpy	2111, 2124, 2148	
phen	2113, 2125, 2149	1993 (X) 2089, 2139, 2161 (Z) (2127, 2158) (Z')

Acknowledgement

This work was supported by the EPSRC (Fellowships to PP and JAW). We thank Dr G. Greetham for his assistance.

References

1. Filippou, A. C.; Portius, P.; Neumann, D. U.; Wehrstedt, K.-D., *Angew. Chem. Int. Ed.* **2000,** 39, 4333-6.
2. Filippou, A. C.; Portius, P.; Schnakenburg, G., *J. Am. Chem. Soc.* **2002,** 124, 12396-7.
3. Portius, P.; Filippou, A. C.; Schnakenburg, G.; Davis, M.; Wehrstedt, K.-D., *Angew. Chem. Int. Ed.* **2010**, in press.
4. Steinhauser, G.; Klapoetke, T. M., *Angew. Chem. Int. Ed.* **2008,** 47, 2-20.
5. Portius, P.; Clark, I. P.; Towrie, M., *Central Laser Facility Annual Report* **2008-2009**, 180-182.
6. Towrie, M.; Grills, D. C.; Dyer, J.; Weinstein, J. A.; Matousek, P.; Barton, R.; Bailey, P. D.; Subramaniam, N.; Kwok, W. M.; Ma, C.; Phillips, D.; Parker, A. W.; George, M. W., *Applied Spectroscopy* **2003,** 57, 367-380.
7. Greetham, G. M.; Matousek, P.; Robinson, D. A.; Parker, A. W.; M.Towrie; Farrow, R. C.; Codd, P. S.; Xin, Z. J.; Goerge, M. W., *CLF Annual Report* **2007-2008**.

Contact *conor.long@dcu, mary.pryce@dcu.ie,*

E. C. Harvey, J. C. Manton, C. Long, M. T. Pryce

School of chemical Sciences, Dublin City University, Dublin 9, Ireland

I. P. Clark, G. M. Greetham, A. W. Parker

Central Laser Facility, STFC, Rutherford Appleton Laboratory, HSIC, Didcot, Oxon 0X11 OQX, UK

Introduction

Organometallic complexes have found many applications in organic syntheses. For instance, coordination of an arene unit to a $M(CO)_3$ (M = Cr or Mo) fragment can activate the arene toward a variety of reactions.[1] Cobalt complexes, such as (μ_2-alkyne)$Co_2(CO)_6$ have been widely used in the Pauson-Khand reaction.[2] The PKR is a versatile route to the synthesis of natural products and pharmaceutically active compounds.[3] We have recently demonstrated that the Pauson-Khand can be driven using visible light irradiation at ambient temperatures.[4]

(η^6-Benzene)$Cr(CO)_3$

The photochemistry of (η^6-Benzene)$Cr(CO)_3$ has been investigated since the early days of flash photolysis[5,6] and matrix isolation.[7] Our recent TRIR studies in room temperature *n*-heptane identified a vibrationally cold excited state as the precursor to CO expulsion to form (η^6-Benzene)$Cr(CO)_2$.[8] This process is comparatively slow, taking place over the course of 150 ps ($\lambda_{exc.}$ = 400 nm).

Within 1 ps of excitation pulse the two ν_{CO} bands of the parent (η^6-Benzene)$Cr(CO)_3$ complex at 1984 and 1916 cm^{-1} were depleted and two broad features formed, at ~ 1965 and 1887 cm^{-1} assigned to the excited state species, [(η^6-Benzene)$Cr(CO)_3$]*. This species is formed with excess vibrational energy. Within 3 ps the bands become narrow and the ν_{CO} bands of "cold" [(η^6-Benzene)$Cr(CO)_3$]* appear at 1965 and 1887 cm^{-1}. The rate of this process was found to be 1.6 (± 0.3) × 10^{12} s^{-1} at 298 K.

The effect of temperature change on this process (274 to 302 K) yielded an activation enthalpy ($\Delta H^{\neq}$) of -10 (± 4) kJ mol^{-1}, suggesting a barrierless process. The activation entropy ($\Delta S^{\neq}$) is -50 (± 16) J mol^{-1} K^{-1} .

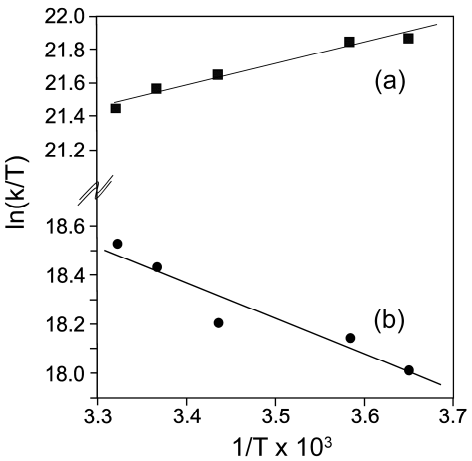

Figure 2. Eyring plots for (a) the growth of the absorption band at 1887 cm^{-1} i.e. the cold excited state and plot (b) was obtained from the growth of the 1872 cm^{-1} band of (η^6-Benzene)$Cr(CO)_2$ (**3**).

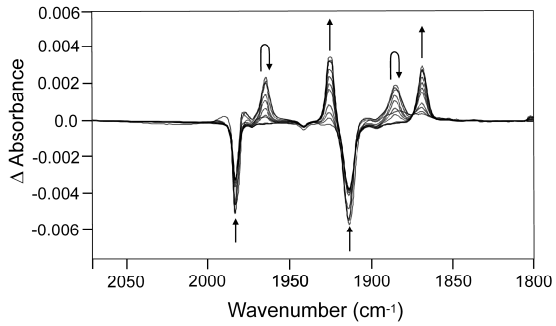

Figure 3. The TRIR spectra obtained following 400 nm excitation of (η^6-Benzene)$Cr(CO)_3$ in *n*-heptane, spectra were recorded at 1, 7, 12, 21, 51, 70, 106, 160, 350, 500, 750, 1000 ps after the excitation pulse. Arrows indicate the time-dependent behavior of the absorption features.

During the subsequent 150 ps, [(η^6-Benzene)$Cr(CO)_3$]* decays with the concomitant formation of (η^6-Benzene)$Cr(CO)_2$ and reformation of (η^6-Benzene)$Cr(CO)_3$. (η^6-Benzene)$Cr(CO)_2$ has ν_{CO} bands at 1927 and 1872 cm^{-1}. It appears that formation of the CO-loss species occurs mainly from the "cold" excited state as does regeneration of (η^6-Benzene)$Cr(CO)_3$ (Scheme 1).

Eyring plots for the formation of (η^6-Benzene)$Cr(CO)_2$ gave $\Delta H^{\neq}$ and $\Delta S^{\neq}$ values of +12 (±4) kJ mol^{-1} and -4 (±7) J mol^{-1} K^{-1} respectively.

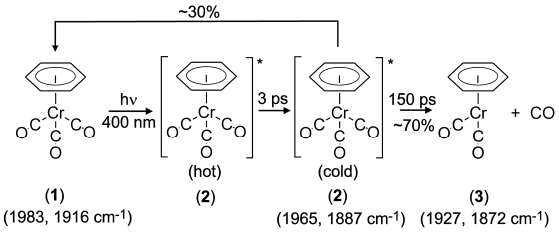

Scheme 1 The excitation of (η^6-Benzene)$Cr(CO)_3$ produces a vibrationally hot excited state. This cools over 3 ps to a vibrationally relaxed excited state which looses CO and relaxes to (η^6-Benzene)$Cr(CO)_3$ over 150 ps.

(η^6-Allylbenzene)$Cr(CO)_3$

(η^6-arene)$Cr(CO)_3$ and (cyclopentadienyl)$Mn(CO)_3$ are of interest in the design of ultrafast photoswitches.[9] When the arene ligand contains a substitutent with a functional group capable of coordinating to an electron deficient 16 electron CO-loss species, the CO-loss species undergoes a subsequent reaction with the pendant substituent to form a "chelate" species (Scheme 2).

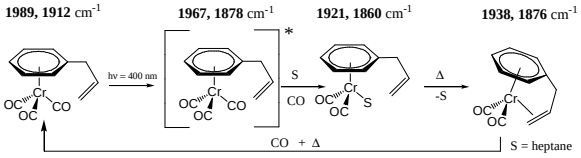

Scheme 2

The TRIR data obtained following photolysis of (η^6-allylbenzene)$Cr(CO)_3$ are presented in Figure 4. Two excited state species are generated. The species at 1967 and 1878 cm^{-1} decays (1.47 x 10^{-12} s^{-1}) to generate the CO loss species (D). This subsequently forms the chelate species (C).

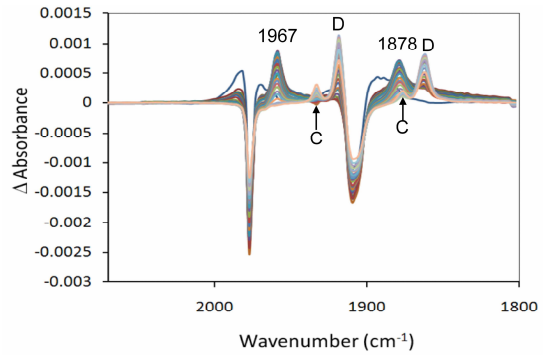

Figure 4 The TRIR spectra obtained following 400 nm excitation of (η^6-allylenzene)$Cr(CO)_3$ in *n*-heptane.

(μ_2-Alkyne)$Co_2(CO)_6$ complexes

The last section of this report deals with the photochemistry of acetylene cobalt carbonyl compounds. Irradiation of diphenylacetylene$Co_2(CO)_6$ at 400 nm in THF resulted in depletion of the parent bands and the formation of bands at 2074, 2041 and 1992 cm^{-1}, which underwent vibrational relaxation within 10 ps. The product species was assigned to the triplet diradical which rapidly reacts within 80 ps, to regenerate the parent complex. No evidence for CO loss was obtained for any of the complexes in Figure 5. The photochemistry of complexes **1-3** was independent of the solvent used (pentane, THF, acetonitrile, or DCM)

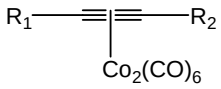

1 R_1 = phenyl, R_2 = phenyl
2 R_1 = phenyl, R_2 = thienyl
3 R_1 = ferrocene, R_2 = H

Figure 5. (μ_2-alkyne)$Co_2(CO)_6$ complexes studied previously

The aim of this study was to increase the efficiency of the CO loss pathway, and to improve their use as CO-releasing molecules (CORMs). Some of the complexes investigated are shown in Figure 6.

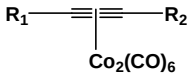

R_1 = pyrene, R_2 = H
R_1 = pyrene, R_2 = ferrocene

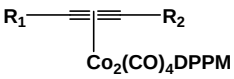

R_1 = pyrene, R_2 = H
R_1 = pyrene, R_2 = ferrocene

Figure 6. (μ_2-alkyne)$Co_2(CO)_6$ complexes studied.

As previously all (μ_2-2-pyrenylacetylene)$Co_2(CO)_6$ and (μ_2-2-pyrenylacetylene)$Co_2(CO)_4(DPPM)_2$ complexes gave rise to the triplet diradical species, ^{3}(μ_2-2-pyrenylacetylene)$Co_2(CO)_6$ or ^{3}(μ_2-2-pyrenylacetylene)$Co_2(CO)_4(DPPM)_2$ with lifetimes between 26 and 78 ps. However the CO loss species, (μ_2-2-pyrenylacetylene)$Co_2(CO)_5$(solvent) was also observed following irradiation of both (μ_2-pyrenylacetyleneferrocene)$Co_2(CO)_6$ and (μ_2-pyrenylacetylene)$Co_2(CO)_6$ (Figure 7). The CO loss species for the latter has ν_{CO} bands at 2074, 2030, 2007, and 1975 cm^{-1}, consistent with literature values. Infrared bands for this CO-loss species remain on the nanosecond timescale, and the parent bands do not fully recover on this timescale.

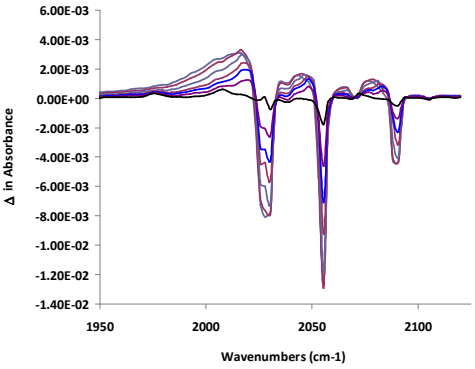

Figure 7. The TRIR spectra obtained following 400 nm excitation of (μ_2-pyreneacetylene)$Co_2(CO)_6$ in *n*-heptane, at 5, 10, 15, 40, 60, 100 and 1000 ps.

Conclusions

The results presented here confirm that photo-induced CO-loss from (η^6-Benzene)$Cr(CO)_3$ occurs via a vibrationally relaxed excited state over a small enthalpy barrier caused by the avoided crossing of two excited state surfaces.

In the case of the (μ_2-alkyne)$Co_2(CO)_6$ and (μ_2-alkyne)$Co_2(CO)_4(DPPM)_2$ complexes, both give rise to a triplet diradical species following irradiation. These react rapidly to regenerate the parent complex in < 80 ps. Photoinduced CO loss was observed following irradiation of both (μ_2-2-pyrenylacetylene)$Co_2(CO)_6$ and (μ_2-2-pyrenylacetyleneferrocene)$Co_2(CO)_6$ complexes.

Acknowledgements

MTP, ECH and JCM acknowledge funding from Science Foundation Ireland (08/RF/PHY082) and the Environmental Protection Agency (2008-ET-MS-3-52). The authors also thank the Central Laser Facility for granting access to the ULTRA system under EU Access grant No.92004.

References

1. McQuillin, F. J.; Parker, D. G.; Stephenson, G. R. *Transition metal organometallics for organic synthesis*; Cambridge University Press: Cambridge UK, 1991.
2. Ojima, I.; Tzamarioudaki, M.; Li, Z.; Donovan, R. J., *Chem. Rev*., **1996**, *96*, 635.
3. Magnus, P.; Principe, L. M., *Tetrahedron Lett.* **1985**, *26*, 4851.
4. Coleman, A. C.; Long, C.; Feringa, B. L.; Browne, W. R.; Pryce, M. T., *Dalton*, **2009**, *38*, 7885.
5. Gilbert, A.; Kelly, J. M.; Budzwatt, M.; Koerner von Gustorf, E. *Z. Naturforsch.* **1976**, *31(b)*, 1091.
6. Creaven, B. S.; George, M. W.; Ginzburg, A. G.; Hughes, C.; Kelly, J. M.; Long, C.; McGrath, I. M.; Pryce, M. T. *Organometallics* **1993**, *12*, 3127.
7. Hitam, R. B.; Mahmoud, K. A.; Rest, A. J. *Coord. Chem. Rev.* **1984**, *55*, 1.
8. Alamiry, M. A. H.; Boyle, N. M.; Brookes, C. M.; George, M. W.; Long, C.; Portius, P.; Pryce, M. T.; Ronayne, K. L.; Sun, X. Z.; Towrie, M.; Vuong, K. Q. *Organometallics* **2009**, *28*, 1461.
9. (a) Yeston, J. S.; To, T. T.; Burkey, T.J.; Heilweil, E. J., *J. Phys. Chem. B*, **2004**, 108, 4582. (b) To, T. T.; Heilweil, E. J.; Duke, C. B. ; Burkey, T. J., *J. Phys. Chem.* A, **2007**, 111, 6933

Excited-State Dynamics of Adenine Thymine Dinucleotides: Influence of Stacking

Contact *susan.quinn@ucd.ie*

S. J. Quinn

School of Chemistry and Chemical Biology, University College Dublin, Dublin 4, Ireland

G. W. Doorley, M. Wojdyla, D. M. McGovern, J. M. Kelly

School of Chemistry, Trinity College Dublin, Dublin 2, Ireland

M. Towrie and A.W Parker

Central Laser Facility, Rutherford Appleton Laboratory, Harwell Science & Innovation Campus, Didcot, OX11 0QX

Introduction

The DNA double helix contains the information required for replicating life; molecular interrogation of the structure through transcription and translation relating it to function. The integrity of this process depends on the stability of DNA and its ability to resist and/or repair erroneous modification. For this reason the study of the excited state dynamics of DNA is of great interest.[1,2,3,4] Through our research we hope gain understanding of the influence of structure on the properties of long-lived excited states achieved through base stacking and hydrogen-bonding interactions and further understand the ultrafast processes that may lead to genetic mutation.

Picosecond ultrafast transient infrared (ps-TRIR) provides structural as well as kinetic information and has been used to study the photodynamics and the photoreactions of mononucleotide and polynucleotide systems.[5,6] Until very recently the singlet excited states of nucleotides were thought to occur on a subpicosecond timescale. However, using ps-TRIR we identified a longer-lived transient state (34 ps) in 5'-dCMP, which had been inferred from transient absorption work by Hare et. al, and provisionally assigned it to the $^1n_N\pi^*$ non-emissive - dark state.[7,8] Our ps-TRIR measurements of the other nucleotides revealed solely information on vibrational cooling.[9] However, polynucleic acids display longer-lived excited states and there is debate regarding the origin of long-lived excited in states and the role of stacking interactions. In this report we present further findings from our psTRIR study of excited state dynamics of the two A-T dinucleotides, namely 2'-deoxyadenyl-(3'-5')thymidine (dApT), and thymidylyl-(3'-5')-2'-deoxyadenosine (TpdA), see Figure 1. These structural isomers exhibit different stacking behaviour in solution and as such were chosen to investigate the role of stacking on the excited state where the nucleic acid components remain constant.

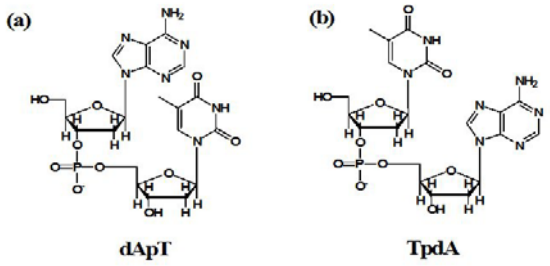

Figure 1: The structure of the two dinucleotide systems studied, (a) dApT and (b) TpdA.

Experimental

Measurements were made using the picosecond infrared absorption and transient excitation (PIRATE) system.[10] The data were collected in a number of 150 cm^{-1} spectral windows using a delay line for optical delays between 2 ps and 1 ns. The difference signal was calibrated using water vapour lines present in the probe spectrum, and the spectral windows were interleaved using overlapping transients recorded at the same delay time. The sample was raster scanned in the x- and y-directions at an approximate rate of 100 mm s^{-1}. The 1-pixel accuracy was ± 4 cm^{-1}. Ground state UV and FTIR measurements were recorded using a Perkin–Elmer Lambda2 and a Nicolet Avatar 360 respectively. Global analysis of the relaxation behaviour was achieved by simultaneous fitting of the transient absorption decay curves at different wavelength using well-known global fitting procedures[11] and assuming a biexponential decay model. Briefly, global fitting with parameter sharing is an option of fitting multiple datasets simultaneously for one function (in this case biexponential decay model). For each shared (global) parameter (in this case lifetime), the one best-fit value that is estimated from all the fitted datasets is obtained.

Results and Discussion

Heterodinucleotide systems: dApT and TpdA

At room temperature the dinucleotides exist in both exist in stacked and unstacked forms in solution (dApT 38% and TpdA 20%).[12] The infra red spectra for both dinucleotides shows bands characteristic of the adenine (ring vibrations ca. 1626 cm^{-1}) and thymine (ring and carbonyl stretches 1629, 1660 and 1684 cm^{-1}), see Figure 2. The ps-TRIR spectrum of dApT following UV excitation is shown in Figure 2a with the shorter delay times (2-10 ps) shown in red and the longer delays (15-1500 ps) shown in black. The spectrum shows bleaches centred at 1623 cm^{-1}, 1661 cm^{-1} and 1694 cm^{-1} and a broad transient spanning from 1530-1612 cm^{-1}. An important feature is the 'tracking' (i.e. shifting of the band to higher wavenumbers) of the transient bands at early times (red delays) and the persistence of bleached and transient bands after 15 ps (black delays) show the presence of a longer-lived species. This is in contrast to what is observed for the constituent mononucleotides, which undergo rapid ground state recovery over 2.2 ± 0.2 ps (5'-TMP) and 4.1 ± 0.4 ps (5'-dAMP). The relative intensity of the individual bands within the bleach region was found to change with time, indicating the presence of more than one species. At early time delays the ratio of the main bleach (1620 cm^{-1}) to the thymine-based bleach (1661 cm^{-1}) is 2:1 but at later times the ratio of the bleaches becomes 1:1 and remains so as the sample relaxes back to the ground state. The kinetic analysis of dApT was carried out using standard global fit analysis of the transients and bleach bands (see experimental section). This showed the presence of two species with lifetimes of 3.9 ± 0.4 ps and 75 ± 7 ps. The first lifetime is characteristic of the monomer species and therefore attributed to the unstacked dinucleotide, while the second lifetime component is attributed to the stacked form of the dinucleotide in solution. The broad absorption band for this longer lived species, which is presumed to be due to an

excited state dimer, is similar to that observed in the polynucleotide {polydA-dT}$_2$.[12]

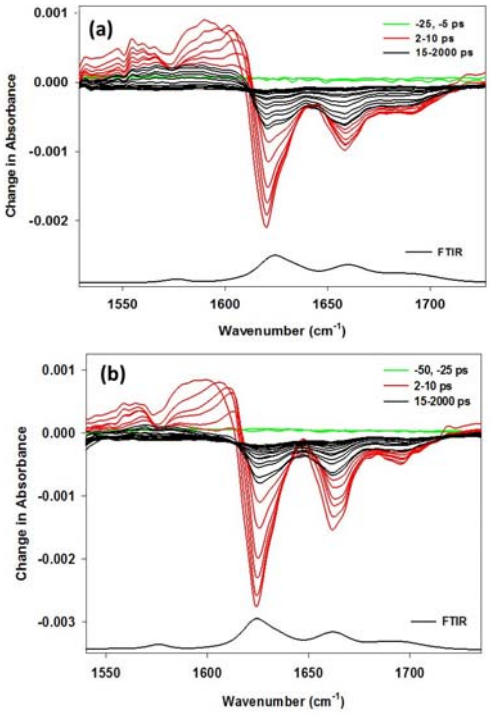

Figure 2: ps-TRIR spectra following UV excitation (300 fs, 267 nm) of 10 mM nucleotide systems in 50 mM potassium phosphate D2O buffer at pH 7, at 20° C. (a) dApT and (b) TpdA. Delays are at –50, -25 (green), 2-10 (red), 15- 2000 ps (black). Below each data set is the FTIR groundstate spectrum taken prior to the ps-TRIR experiment.

The ps-TRIR spectrum of TpdA following UV excitation is shown in Figure 2b. As for dApT the spectrum shows bleaches centered at 1623 cm^{-1}, 1661 and 1694 cm^{-1} and a broad transient spanning from 1530-1612 cm^{-1} are recorded. Again the persistence of the bleached and transient bands after 15 ps indicated the presence of a long-lived species. Again kinetic analysis yielded two lifetimes for recovery of 4.2 ± 0.4 ps and 50 ± 5 ps. The former value is in close agreement to that found for the short-lived species in dApT (3.9 ± 0.4 ps) as would be expected if they arise from the unstacked nucleotides. However, the long-lived species shows a significantly shorter lifetime compared to that of its isomer (75 ± 7 ps). Furthermore, the relative yield of the long-lived transient was determined to be approximately 50 % of that found for dApT, consistent with the smaller amount of stacking in the TpdA isomer. The long-lived species possessed a distinctive spectroscopic signature in the region 1500-1600 cm^{-1}, which is not present in the homodinucleotides, dApdA and TpT. The signature is identical to that of the long-lived state observed in double stranded poly(dA-dT). Indicating that the excitation in the polymer is localized on the dinucleotide unit.

Conclusions

This study illustrates how ps-TRIR can provide valuable insights into the fast photophysical properties of nucleic acids, and so complement the measurements obtained by the more established transient Uv/visible absorption and luminescence methods.[5] In particular it is apparent from this study that stacking of the nucleobases gives rise to a longer-lived species, which possesses a characteristic infra-red band in the 1550 – 1600 cm^{-1} region in the case of the adenine-thymine bases. (The yield of the long-lived transient is greater for dApT than for TpdA reflecting the larger amount of stacked form present at equilibrium in solution.) Takaya et al.[13] recently made femtosecond Uv-vis transient absorption measurements on dinucleotides and assigned long-lived states to purine-pyrimidine charge transfer states. The characteristic signal we observe may therefore be associated with such a charge redistribution in the stacked bases. In this connection we may point out we have also observed that long-lived excimer excited states from adenine homodinucleotides do not show a similar infra-red absorption. Such differences in the spectroscopic signals opens up the prospect of being able to identify localised states in photo-excited DNA – for example, we have previously suggested that other localised states may be identifiable in {polydG-dC}$_2$.[14]

The kinetic measurements firstly reveal the major difference in properties between the stacked and unstacked forms of the dinucleotide, with the unstacked conformers behaving very much like the mononucleotides, which undergo sub-picosecond relaxation to the ground states. The 'hot' ground state formed is observed to deactivate with a lifetime of about 4 ps and as expected the rate of vibrational deactivation does not depend on the isomeric species studied. However there is a difference in the rate of relaxation for the longer-lived excited states of the two AT isomers and these differences in lifetimes appear to correlate with the extent of stacking.

In conclusion this study shows that a study of dinucleotides can be very useful in understanding the role of stacking of the nucleobases, in the absence of H-bonding base-pairing, and as such should be helpful in allowing us to determine the relative significance of intra- and inter-chain processes in double-stranded DNA.[15]

Acknowledgements

We gratefully acknowledge the support of Science Foundation Ireland (Grant numbers 06/RFP/CHP035 and 07/CHEF437). and thank STFC and the EU for access to the PIRATE laser system.

References

1. (a) Middleton, C. T.; de La Harpe, K.; Su, C.; Law, Y. K.; Crespo-Hernández, C. E.; Kohler, B. Annu. Rev. Phys. Chem. 2009, 60, 217-239. (b) Crespo-Hernández, C. E.; Cohen, B.; Hare, P. M.; Kohler, B. Chem. Rev. 2004, 104, 1977-2020.

2.(a) Miannay, F.-A.; Banyasz, A.; Gustavsson, T.; Markovitsi, D. J. Am. Chem. Soc. 2007, 129, 14574-14575. (b) Onidas, D.; Markovitsi, D.; Marguet, S.; Sharonov, A.; Gustavsson, T. J. Phys. Chem. B 2002, 106, 11367-11374.

3. Peon, J.; Zewail, A. H. Chem. Phys. Lett. 2001, 348, 255-262.

4. Pecourt, J. M. L.; Peon, J.; Kohler, B. J. Am. Chem. Soc. 2001, 123, 10370-10378.

5. Towrie, M., Doorley, G. W., George, M. W., Parker, A. W., Quinn S. J., Kelly J. M. ***Analyst***, 2009, **134**, 1265 - 12735.

6. Schreier, W. J.; Schrader, T. E.; Koller, F. O.; Gilch, P.; Crespo-Hernández, C. E.; Swaminathan, V. N.; Carell, T.; Zinth, W.; Kohler, B. *Science* **2007**, *315*, 625-629.

7. Quinn, S.; Doorley, G. W.; Watson, G. W.; Cowan, A. J.; George, M. W.; Parker, A. W.; Ronayne, K. L.; Towrie, M.; Kelly, J. M. Chem. Commun. 2007, 2130-2132.

8. Hare, P. M.; Crespo- Hernández, C. E.; Kohler, B. Proc. Natl. Acad. Sci. 2007, 104, 435-440.

9. Kuimova, M. K.; Dyer, J.; George, M. W.; Grills, D. C.; Kelly, J. M.; Matousek, P.; Parker, A. W.; Sun, X. Z.; Towrie, M.; Whelan, A. M. *Chem. Commun.* **2005**, 1182-1184.

10. M. Towrie, D. C. Grills, J. Dyer, J. A. Weinstein, P. Matousek, R. Barton, P. D. Bailey, N. Subramaniam, W. M. Kwok, C. S. Ma, D. Phillips, A. W. Parker and M. W. George, *Appl. Spec.*, 2003, **57**, 367.

11. Satzger, H.; Zinth, W. *Chem. Phys.* **2003**, *295*, 287-295

12. Cantor, C., R. ; Warshaw, M., M. ; Shapiro, H. Biopolymers 1970, 9, 1059-1077.
13. Takaya, T.; Su, C.; de La Harpe, K.; Crespo-Hernández, C. E.; Kohler, B. Proc Natl Acad Sci U S A Biol Sci 2008, 105, 10285-10290.
14. Doorley, GW, McGovern, DA, George, MW, Towrie, M, Parker, AW, Kelly, JM and Quinn, SJ *Angew. Chem. Int. Ed.* **2009**, 48, 123 –127.
15. Aspects of this work were presented at the Ultrafast Phenomena XVI conference.

Antigens laid bare: the intrinsic conformation of Lewis^x

Contact *John.Simons@chem.ox.ac.uk*

John P. Simons, Zheng Su, Emilio J. Cocinero
Department of Chemistry, Physical and Theoretical Chemistry Laboratory, South Parks Road, Oxford OX1 3QZ, UK

Beat Ernst, Beatrice Wagner
Institute of Molecular Pharmacy, University of Basel, Klingelbergstrasse 50, 4056 Basel, (Switzerland)

Introduction

Lewis^x (Le^x), one of the so-called Type 2 antigens (Le^x, Le^y) presenting the trisaccharide epitope, Galβ1-4[Fucα1-3]GlcNAc, is expressed by many cancers of epithelial origin and is an important immunotherapeutic target. Knowing its structural preference(s), particularly in its bioactive conformation, is a key requirement in designing drugs which might inhibit its binding and activity. Condensed phase environments are known to favour relatively rigid, compact structures with the terminal pyranosides, Gal and Fuc, stacked in parallel and separated – depending on the environment - by approximately 4 to 5Å. Thus structures determined through X-ray diffraction can be stabilised by the protein or crystalline environment and NMR measurements of nuclear Overhauser effects, scalar or residual dipolar couplings in aqueous environments, coupled with MD simulations to provide dynamically averaged structures, can be influenced by explicit hydration and 'water bridging' across the glycosidic linkages. To understand the influence of the environment on the structure of Lewis antigens it is essential to know first, their *intrinsic* conformational landscapes but these have not been determined experimentally. MM and MD calculations have been conducted *'in vacuo'* but their predictions depend on the accuracy of the assumed force fields; *ab initio* calculations of Le^x have also been conducted, but only at a low (Hartree-Fock) level of theory.

The vibrational spectra of individual carbohydrate conformers can be obtained in a cold molecular beam using double resonance IR-UV ion dip spectroscopy (IRID),[1] and by comparing them with those determined through a combination of molecular mechanics, density functional theory (DFT) and *ab initio* calculations it is possible to determine the intrinsic carbohydrate structures experimentally. Following this strategy, the target molecule, Le^x has been synthesized in large scale, as the β-*O*-phenyl glycoside (to provide the necessary UV chromophore required for IRID detection, see Figure 1).

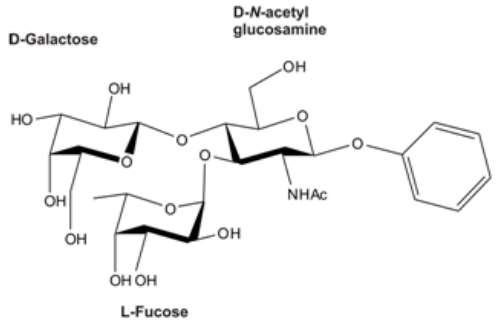

Figure 1. Schematic molecular structure of the antigen, Lewis^X ('tagged' with a phenyl group to facilitate its spectroscopic interrogation).

Results and Discussion.

The computed structures and relative energies of the three lowest lying conformers are presented in Figure 2. The conformer that most closely resembles the 'stacked' structures (of the β-*O*-methyl glycoside) in aqueous solution, in the hydrated crystal and in protein-bound Le^x, does not correspond to the intrinsic global minimum predicted by the calculations but to the conformer calculated to lie at an energy 2.9 kJ mol^{-1} above it, see Figure 3.

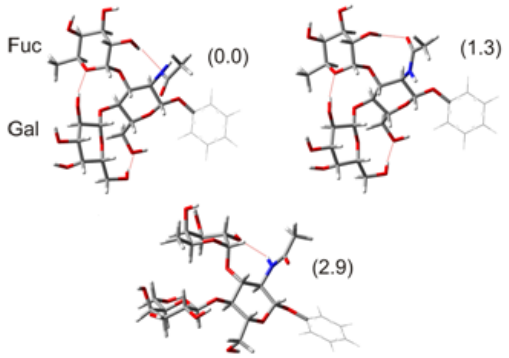

Figure 2. Structures and relative energies, in kJ mol^{-1}, of the three lowest energy conformers of *O*-phenyl Le^x.

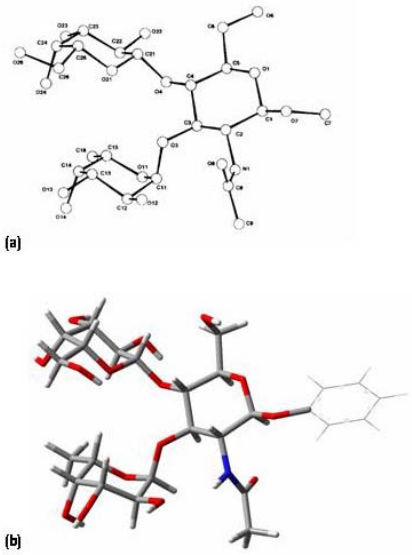

Figure 3. Comparison between (a) the crystal structure of β-*O*-methyl Lewis^x [2] and (b) the computed structure of the 'stacked' conformer, #3, of β-*O*-phenyl Lewis^x

Neither of the two lowest energy conformers displays this type of structure. In the stacked structure, apart from a weak hydrogen-bond between the Glc*N*Ac and Fuc residues, *r*(NH••OH2)=2.18Å, there are no inter-ring hydrogen bonds. This contrasts sharply with the other two structures, both of which display strong inter-ring linkages between all three residues, including: $OH2^{Gal}\rightarrow O5^{Fuc}$, *r*(OH2••O5)=1.83-1.88Å and $OH6^{Gal}\rightarrow O6^{GlcNAc}$, *r*(OH6••O6)=1.99Å. These inter-ring linkages create quite rigid and inflexible structures but the glycosidic structure of the stacked conformer should be rather more mobile. The acetamido group is oriented roughly perpendicular to the 'plane' of the pyranoside ring (dihedral angle, C3-C2-N-H ~ 85°) but the exocyclic CH_2OH groups adopt a 'parallel' *gt* orientation in almost every case apart from the stacked conformer, where there is no inter-ring hydrogen bonding and the orientation of the CH_2OH^{GlcNAc} group is *gg*. Are these predictions in agreement with experiment?

The UV R2PI spectrum of the trisaccharide, vaporized through pulsed laser ablation and entrained in a cold Ar molecular beam, presents a broad, structureless bimodal band centred at ~272 nm but the associated IRID vibrational spectra recorded with the UV probe laser located at different wavelengths within the band contour are all identical, suggesting the population of a single conformer only (unless they have identical UV absorption spectra). This suggestion is reinforced by an analysis of the experimental IRID spectrum, recorded between 3300 cm^{-1} and 3700 cm^{-1} and shown in Figure 4, together with the vibrational spectra predicted for each of the three lowest lying conformers. The experimental spectrum in no way resembles that of the stacked configuration, relative energy 2.9 kJ mol^{-1}, shown in Figure 3 - or those lying at higher relative energies, and it can be firmly excluded. It does resemble, but is in rather poor correspondence with the spectrum of the second conformer, relative energy 1.3 kJ mol^{-1} and the spectrum in closest correspondence with experiment and the only one to predict the closely spaced doublet at 3500-3550 cm^{-1}, is associated with the global minimum conformation. The cluster of OH bands located at high wavenumbers, between ~3570 cm^{-1} and 3650 cm^{-1} can be assigned to the weakly hydrogen-bonded peripheral 'spectator' OH groups. The more intense red-shifted doublet between 3500 cm^{-1} and 3550 cm^{-1}, indicates two moderately hydrogen bonded OH stretch modes, which can be assigned to σ2(*Fuc*) and σ6(*Gal*). The sharp feature at 3455 cm^{-1} is associated with the 'free' NH vibration and the strongly displaced and broadened band centred ~3430 cm^{-1}, which indicates a strongly hydrogen bonded OH group, can be assigned to the vibrational mode, σOH2(*Gal*).

These results confirm the theoretical predictions and reveal a clear distinction between the *intrinsic* conformational preference of Le^x, *'in vacuo'* and the preferences established in aqueous, hydrated crystalline or protein-bound environments. They also present a conundrum. In the condensed phase, all the experimental evidence points to the adoption of a rather rigid, compact stacked conformation, despite the absence of intramolecular hydrogen bonding across the glycosidic linkages. In the gas phase these linkages do provide rigidity but the intrinsic molecular conformation does not correspond to the stacked configuration. In aqueous solution and as a bound ligand, the CH_2OH(*Gal*) orientation is *gt*, but in the gas phase it is *gg*. Some involvement of the aqueous environment is evidently implicated. Stabilisation of the higher energy stacked configuration is unlikely to be promoted by the solvent polarity since its calculated dipole moment, 2.6 Debyes, is much smaller than that of the global minimum conformation populated in the gas phase, 7.2 Debyes. Instead the preference for the stacked conformation in aqueous environments and its rigidity must be associated with the replacement of intramolecular hydrogen bonding by explicit hydration or 'bridging events' – in agreement with recent predictions made for the Lewis antigens on the basis of MD simulations using the GLYCAM04 force field [3] and more broadly for oligosaccharides in general.The new gas phase results reported here, for Le^x, also imply a key structural role for an aqueous environment, including perhaps hydrophobic and electrolytic interactions, in controlling the conformation of Le^x and in consequence, its biological function.

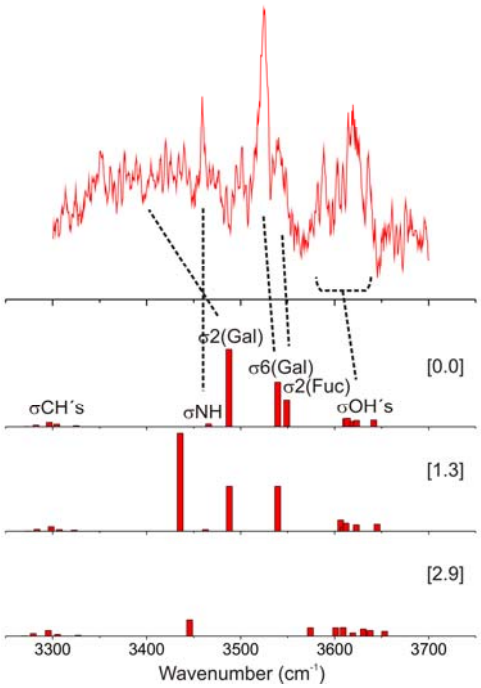

Figure 4. The experimental IRID spectrum of β-*O*-phenyl Le^x (upper trace) and the computed vibrational spectra of its three lowest energy conformers; relative energies (kJ mol^{-1}) shown in brackets.

Conclusions

The conformation of the $Lewis^x$ antigen has been determined, free of environmental perturbation, at low temperature in the gas phase to reveal a global minimum energy structure lying below the rigid stacked conformations adopted in aqueous solution, in the crystalline hydrate or when bound to proteins. The result suggests that water plays a key structural role in controlling the conformation of $Lewis^x$ and in consequence, its biological function.

Acknowledgements

Financial support was provided by the EPSRC (Grant GR/T26542), the Leverhulme Trust (Grant F/08788G), NSERC Canada (ZS), and the Swiss National Science Foundation (200020-120628). Additional support was provided by the STFC Laser Support Facility, the Oxford Supercomputing Centre and the Physical and Theoretical Chemistry Laboratory.

References

1. J. P. Simons, R. A. Jockusch, P. Çarçabal, I. Hünig, R. T. Kroemer, N. A. Macleod and L. C. Snoek, Intl. Rev. Phys. Chem. 24 (2005) 489.
2. F. Yvelin, Y-M Zhang, J-M. Mallet, F. Robert, Y. Jeannin, P. Sinaÿ, Carbohydrate Lett. 1 (1996) 475.
3. M. Reynolds, A. Fuchs, T. K. Lindhorst, S. Pérez, Molecular Simulation 34 (2008) 447.

Carbohydrate molecular recognition: probing CH-π interactions

Zheng Su, Emilio J Cocinero and John P Simons

University of Oxford
Physical and Theoretical Chemistry Laboratory, South Parks Road, Oxford OX1 3QZ (UK)

Benjamin G Davis

University of Oxford
Chemistry Research Laboratory, Mansfield Road, Oxford OX1 3TA, UK

E Cristina Stanca-Kaposta

Free University Berlin
Institut für Experimentalphysik, Freie Universität Berlin, Arnimallee 14, 14195, Berlin, (Germany)

Main contact email address: *John.Simons@chem.ox.ac.uk*

Introduction

Molecular recognition of carbohydrates by proteins often involves their selective binding at sites adjacent to aromatic amino acid residues and X-ray crystallographic measurements have revealed a stacked, "apolar CH-π bonding" motif, with the aromatic side group providing a platform for the bound ligand. "Hydrophilic" OH-π hydrogen bonded interactions have also been inferred from the crystallographic data. IR ion dip (IRID) spectroscopy of O-H vibrational modes has been used in small model carbohydrate-aromatic systems isolated in the gas phase and free of neighbouring water molecules, to provide a more direct experimental probe of intermolecular bonding since their frequencies and intensities are extraordinarily sensitive to their local inter (and also intra) molecular hydrogen bonded environments. OH-π hydrogen bonding was signaled by a red-shift, broadening and intensification of one (or more) of the O-H bands.[1] The *absence* of any significant displacement of the OH modes in an aromatic complex was taken as an indirect indication of carbohydrate binding through "CH-π" interactions, provided the OH-π interaction was stronger than any pre-existing OH-O interaction with a neighbouring OH group; (the operation of CH-π interactions did not necessarily preclude a minor contribution from OH-π bonding as well).

Similar spectroscopic measurements of shifts in the IR frequencies of the C-H modes between free and bound carbohydrates, which might be used to 'report' directly on the incidence of CH-π bonding in their aromatic complexes, have not been undertaken. The observation of specific displacements might, with the aid of predictive quantum chemical calculations, help in their structural assignment since the magnitude and direction of the spectral shifts that can be associated with CH-π bonding have been intensively discussed in recent years, particularly the information they may convey about the nature of the interaction.

Two complexes which had previously been associated with CH-π, rather than OH-π bound structures because of the absence of any significant change in the OH spectrum of the bound carbohydrate, included methyl α-D-galactopyranoside•toluene (MeGal•Tol) and its 6-deoxy analogue, methyl α-L-fucopyranoside•toluene (MeFuc•Tol), see Figure 1; (the enantiomeric choices reflect Nature's preferences). These experiments have now been extended using MeFuc•Tol as a benchmark system and toluene-d_8, to obtain the IR spectrum of the bound carbohydrate in the CH stretch region without spectral interference from its aromatic partner. At the same time DFT calculations have been conducted for both the isolated and the complexed carbohydrate, using Zhao and Truhlar's MO5-2X functional[2] (which takes proper account of electron exchange and correlation) and the predictions have been compared with experiment, both for the OH spectra reported earlier and for the newly recorded CH spectra.

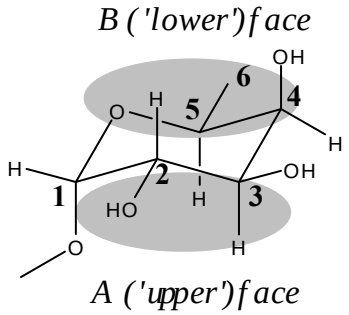

Figure 1. Schematic structure of methyl α-L-fucopyranoside (MeFuc)

Results and Discussion

The lowest lying structures (<10 kJ mol^{-1} above the minimum) of MeFuc•Tol-d_8 calculated using the MO5-2X functional are listed, together with their relative energies and binding energies, in Table 1. 'CH_i-π' or 'OH_i-π' identify the character of the intermolecular interaction with the aromatic partner. Seven of the eight calculated structures are bound through CH-π interactions, leading to binding energies in the range ~(13 – 18) kJ mol^{-1}. The only one involving an OH-π hydrogen bond has the highest relative energy, 7.6 kJ mol^{-1} and the rest involve binding either at the CH_1 site, which is located on the lower face of the pyranoside ring (see Figure 1) or the $CH_{3,4}$ site which binds the fucose to an apolar patch on the upper face of the ring. Both types of interaction have been identified in X-ray crystallographic investigations of complexes between proteins and methyl α-L-fucopyranoside (MeFuc).

structure	ΔE	ΔE+ZPE	D_0
CH_1-πa	0.00	0.00	-22.06
CH_1-πb	2.70	1.49	-20.57
CH_1-πc	2.96	1.73	-20.33
$CH_{3,4}$-π	3.96	2.41	-19.65
CH_1-πd	3.07	3.62	-18.45
CH_2-π	5.42	4.63	-17.43
CH_1-πe	7.66	5.98	-16.09
OH_2-π	9.22	7.61	-14.46

Table 1. Relative energies and binding energies in kJ mol^{-1}, of the eight lowest energy structures of MeFuc•Tol-d_8 calculated using the MO5-2X functional and a 6-31+G** basis set. The 'πa,b,……' notation identifies different orientations of the aromatic ring, which differ only by rotation in the aromatic plane.

Figure 2 compares the computed OH vibrational spectra of the *un*complexed carbohydrate (fig. 2a) with the experimental IRID OH spectrum of the complex, which populates two alternative

structures, or structural families, (fig. 2b) and the OH vibrational spectra associated with the lowest energy structures of MeFuc•Tol-d_8, CH_1-π (figs.2c-e) and $CH_{3,4}$-π (fig. 2f), calculated using the MO5-2X functional. They are all very similar although the CH-π interactions do lead to very minor changes in the spectral patterns. Apart perhaps, from the minimum energy structure, each one of them is in good correspondence with each of the experimental spectra (though this is *not* true for the OH spectra associated with any of the calculated higher energy structures). It is tempting to associate the two experimental spectra with CH_1-π and $CH_{3,4}$-π bonded structures.

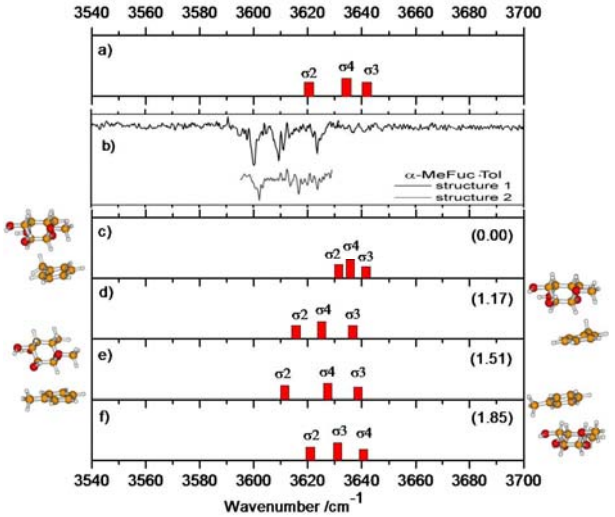

Figure 2. (a). Computed OH vibrational spectrum of methyl α-L-fucopyranoside; (b) IRID OH spectra (shown as 'dip' spectra) of the two populated conformers of MeFuc•Tol-d_8 and (c) – (f), the corresponding vibrational spectra and conformations of its lowest lying computed structures.

Similar comparisons conducted in the CH spectral region are presented in Figure 3, which presents the computed vibrational spectra of uncomplexed MeFuc and the four lowest energy MeFuc•Tol-d_8 structures, and the experimental IRID spectrum associated with the more strongly populated complex ('structure 1' in Fig. 2b). Disappointingly, all the spectra are qualitatively similar and this, when coupled with their complexity and the poor resolution and intensity of the experimental spectrum, prevents assignment of the complex to a particular structure or the vibrational assignment of its experimental spectrum. Comparisons between the computed spectra of each of the complex structures and the bare carbohydrate do however, reveal some interesting results. Each of the spectra shown in Figures 3c-3e is associated with a structure bound through a C_1H-π interaction; when they are compared with the spectrum of bare MeFuc, 'blue shifts' can be identified in the respective C_1-H bands ~35 cm^{-1} (c), ~64 cm^{-1} (d) and ~57 cm^{-1} (e) but none of the other bands is significantly displaced. Similarly, the C_3-H and C_4-H bands in spectrum (f), which is associated with a $C_{3,4}$-π bound complex, are blue-shifted by ~30 cm^{-1} and ~66 cm^{-1} respectively, but not the other bands which are virtually unaffected. These large, selective displacements towards higher wavenumber are comparable in magnitude (and direction) with those calculated for similar CH-π bonded carbohydrate-toluene structures, using the dispersion corrected D-DFT method.[3] Remarkably, blue shifts (about one third as large) are also predicted by calculations using the B3LYP functional although it is not capable of dealing with dispersive interactions.

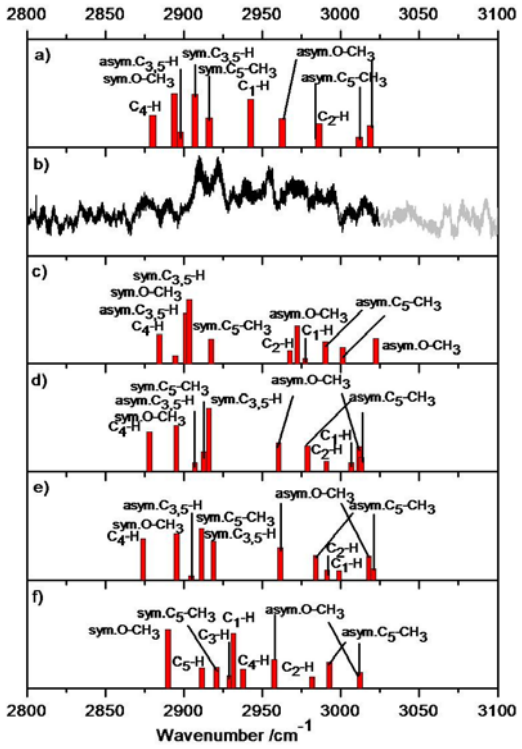

Figure 3. (a). Computed CH vibrational spectrum of methyl α-L-fucopyranoside; (b) IRID CH spectra of conformer 1 of MeFuc•Tol-d_8; (c) – (f) corresponding vibrational spectra of its lowest lying computed structures. (The weak features lying above ~3025 cm^{-1} are due to aromatic C-H bands associated with a small population of undeuterated toluene clusters).

Conclusions

The aromatic molecule is evidently bonded to the upper or the lower face of the pyranoside ring, through $CH_{3,4}$-π (upper) or CH_1-π (lower) interactions. The theoretical prediction of a strong blue shift in the CH bands associated with the CH-π interactions parallels[3] the predictions made recently, on the basis of D-DFT calculations for other carbohydrate-toluene complexes,[4] and encourages a further experimental pursuit based upon a simpler benchmark system, e.g. the xylose-toluene complex, methyl α/β-D-xylopyranoside-toluene-d_8, which provides an analogue of glucose rather than galactose since all its OH groups adopt an equatorial orientation. If the methoxy group were fully deuterated, the number of CH bands would be almost halved to allow a considerable spectral simplification.

Acknowledgements

Dr Timothy Vaden has provided helpful comments and Mr James Screen performed early measurements and calculations. Financial support has been provided by EPSRC, the Leverhulme Trust (JPS, Grant F/08788G), and NSERC (ZS). Support has also been provided by the Oxford Supercomputing Centre.

References

1. E.C. Stanca-Kaposta, D.P. Gamblin, J. Screen, B. Liu, L.C. Snoek, B.G. Davis and J.P. Simons, *Phys. Chem. Chem. Phys.* 2007, **9**, 4444.

2. Y. Zhao and D.G. Truhlar, *J. Chem. Theor. Comput.* 2007, **3**, 289.

3. Z. Su, E.C.Stanca-Kaposta, E.J. Cocinero; B.G. Davis and J. P. Simons, *Chem. Phys. Letters* 2009, **471**, 17.

4. R.K. Raju, A. Ramraj, M.A. Vincent, I.H. Hillier and N.A. Burton, *Phys. Chem. Chem. Phys.* 2008, **10**, 6500.

Polymer coil-globule transition dynamics on the nanosecond to second time scale

Contact *m.volk@liv.ac.uk*

Christopher Bentley and Martin Volk
Surface Science Research Centre, University of Liverpool, Liverpool L69 3BX, UK

Johannes Magnusson and Cameron Alexander
School of Pharmacy, University of Nottingham, Nottingham, NG7 2RD

Introduction

Poly(N-isopropylacrylamide) (pNIPAm, Fig 1) undergoes a change in conformation from a hydrated random coil to a partially dehydrated globular structure when heated over the lower critical solution temperature (LCST). Aggregation of the globules due to hydrophobic interactions and intermolecular hydrogen bonds then leads to phase separation. Applications of this effect include thermally or pH switchable drug or DNA delivery and control of enzymatic activity.[1]

This phase transition has been studied extensively; however, the *dynamics* of the transition has received only little attention so far. The temperature-jump (T-jump) induced coil-globule dynamics of cross-linked pNIPAm gel nanoparticles have been reported to occur on the 100 ns time scale,[2] but dynamics of the single chain polymer phase transition are still in question.[3]

We use laser-induced T-jumps and IR spectroscopy to follow the polymer collapse. We report evidence for fast local collapse of the polymer, but very slow phase separation in single chain pNIPAm samples. On the other hand, phase separation occurs on the 100 ms time scale at concentrations resulting in significant overlap of the polymers in the coil state.

Experimental

PNIPAm polymer (M_n ~20,000) was synthesized by standard methods, dissolved in D_2O and placed in a temperature-controlled IR cell with CaF_2 windows and 50 µm pathlength. The pNIPAM LCST was confirmed to be at 35°C by UV-vis spectroscopy. FTIR spectra were corrected for D_2O absorbance.

T-jumps were induced with visible laser light using co-dissolved heat transducers which absorb the laser energy and rapidly convert it to heat; here, either gold nanoparticles or the dye Basic Red were used. For measurements on the ns-time scale, a pulsed Nd:Yag laser (532 nm, 1 mJ) is used to heat the sample within 5 ns. The accessible time window in this case is limited to less than 1 ms due to cooling by thermal diffusion. For accessing longer time scales, an Ar-ion laser (1 W at 514.5 nm) was used. After a fast shutter turns on the laser beam within 1 ms, the irradiated volume warms up and reaches thermal quasi-equilibrium on the time scale of 10 ms, Fig. 3A, limited by the speed of thermal diffusion. In both cases, the IR absorbance of the polymer solution was followed using a tunable cw lead-salt diode IR laser and a fast MCT IR-detector (rise time 20 ns).

The size of the T-jump was determined from the absorbance change at 1584 cm^{-1}, which is due to the shift of the D_2O association band with temperature, whereas the polymer absorbance at this wavelength is small and shows no change with temperature (Fig. 1A); comparison with FTIR spectra of D_2O allows direct calibration of the temperature change.

Results – Temperature Dependent FTIR Spectra

FTIR spectra of the amide I' band, which is dominated by the amide-carbonyl stretch vibration, taken at incremental temperatures around the LCST, are shown in Fig. 1A. The position of this band responds strongly to changes of the polymer conformation. Below the LCST, pNIPAM exists as a hydrated coil, and the amide I' band is dominated by a band at 1625 cm^{-1} due to carbonyls hydrogen bonded (H-bonded) to water. Above the LCST, part of the amide I' band shifts to 1650 cm^{-1} due to intramolecular (amide-amide) H-bonds.[4] Spectral deconvolution shows a significant contribution of a band at 1610 cm^{-1}, which can be ascribed to carbonyls bound to water molecules trapped in collapsed polymer sections. The fraction of carbonyls which are hydrated, form intramolecular H-bonds or are H-bonded to trapped water can be estimated from the band areas obtained from the fits, Fig. 1B. There is a small loss of freely hydrated carbonyls and increase of trapped water with increasing temperature even below the LCST, indicating the increased formation of locally collapsed polymer sections (see below). At the LCST, larger structural changes occur, including the formation of intermolecular H-bonds as the chains collapse and phase-separate.

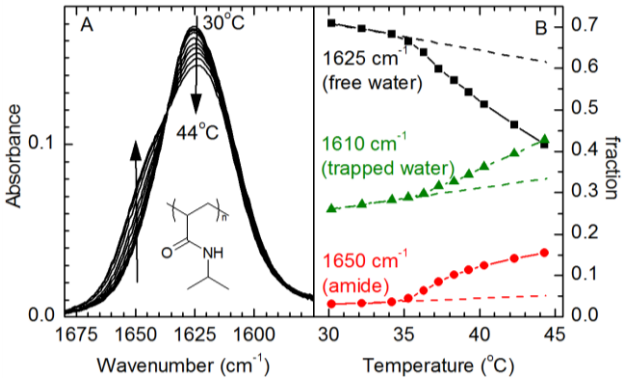

Fig 1. (A) FTIR spectra in the amide I' region of pNIPAm (10mg/ml in D_2O; inset shows chemical structure, n~200) at temperatures around the coil-globule transition (30-44°C), arrows indicate increasing temperature. (B) Fraction of the three component bands obtained from spectral deconvolution with pseudo-Voigt bands, see text for details.

Results - Nanosecond Dynamics

Fig. 2 shows time-dependent IR absorbance changes following a T-jump over the LCST. The size of the T-jump was determined from the signal at 1584 cm^{-1}, which is due to D_2O, as described above. The absorbance recovery at 1584 cm^{-1} on the 100 µs-time scale indicates cooling due to thermal diffusion. The absorbance at 1622 cm^{-1}, which has a contribution from the polymer, also decreases instantaneously within our time resolution and then remains constant in the window of ~1 ms accessible by our ns-setup, following the 1584 cm^{-1} absorbance changes exactly, Fig. 2. However, the absorbance change at 1622 cm^{-1} is larger than that at 1584 cm^{-1}, although D_2O has a smaller temperature-induced absorbance change at this wavelength; this shows that there is an instantaneous bleach of the polymer absorbance. The observed polymer absorbance change agrees well with that predicted from the temperature-dependent FTIR spectra by extrapolating the sub-LCST temperature dependence to temperatures above the LCST (dashed lines in Fig. 1B). As discussed in more detail below, this indicates that a T-jump-induced *local* collapse of PNIPam occurs within a few ns.

On the other hand, the 1622 cm^{-1} absorbance change on the ns-time scale is smaller than the overall change predicted from the FTIR spectra. This shows that a second slower phase of relaxation, namely aggregation and phase separation, is too slow (slower than 1 ms) to be observable in these measurements.

Results – Millisecond Dynamics

Measurements on the time scale 10 ms to 5 s are shown in Fig. 3. At a concentration of 10 mg/ml, Fig. 3A, the results for 1584 cm^{-1} are identical to those obtained in the absence of polymer and thus provide a direct measure of the temperature after turning on cw irradiation. The LCST is reached after 10 ms; within 100 ms 90% of the final T-jump has been reached. At 1622 cm^{-1}, a larger absorbance decrease is found which is in full agreement with the results on the 10 ns-time scale (Fig. 2) when taking into account the slightly different experimental conditions. Again, the time dependence of the absorbance changes at the two wavelengths is identical, indicating that even in this longer time window no major structural changes occur after the initial local collapse. Additionally, we obtained the absorbance change at 1641 cm^{-1}, where the bleach of the D_2O absorbance is partly compensated by an absorbance increase of the polymer. These results are also fully compatible with local collapse only.

Completely different results are obtained at a concentration of 45 mg/ml, however (Fig. 3B). Here, the same instantaneous absorbance change due to local collapse is found (accounting for larger polymer absorbance at the higher concentration). After an induction period of 200 - 400 ms, however, significant changes of the absorbance at all wavelengths occur with a time constant of ~500 ms. The same results were obtained for concentrations in the range 30 - 100 mg/ml. Most interestingly, these absorbance changes cannot arise from structural changes of the polymer, since the polymer absorbance decreases both at 1622 cm^{-1} and 1641 cm^{-1}, whereas at 1584 cm^{-1}, where the polymer does not have any significant absorbance at all, it increases. These observations allow only one conclusion, namely that polymer is removed from the probed volume (decreasing amide I' absorbance) and is being replaced by water (increasing absorbance at 1584 cm^{-1}); the size of the observed effects is consistent with ~15% of the polymer being replaced by water.

Discussion

Cooperative hydration, which results in a "pearl-necklace" type chain conformation with locally collapsed polymer globules even below the LCST, has been suggested as the mechanism behind the pNIPAm coil-globule transition. Theoretical considerations predict an increase of the number and/or size of locally collapsed polymer sections with increasing temperature even below the LCST.[5] This is fully confirmed by our FTIR spectra, which show a decreasing fraction of normally hydrated carbonyls and increasing number of carbonyls bound to trapped water with increasing temperature below the LCST (Fig. 1B).

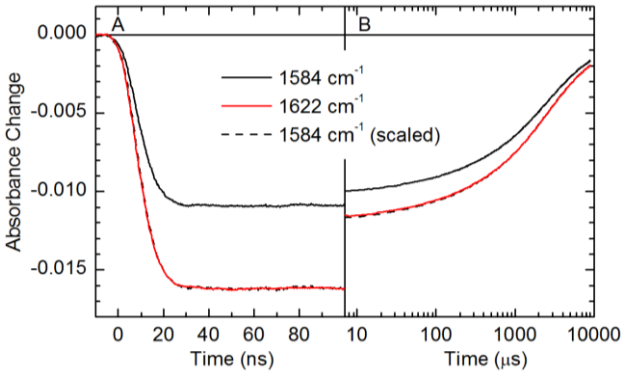

Fig 2. Absorbance changes of a pNIPAm sample in D_2O on the time scale 10 s to 1 ms. (A) 20 mg/ml, T-jump from 32 °C to 37.5°C; (B) 7 mg/ml; T-jump from 32°C to 37°C.

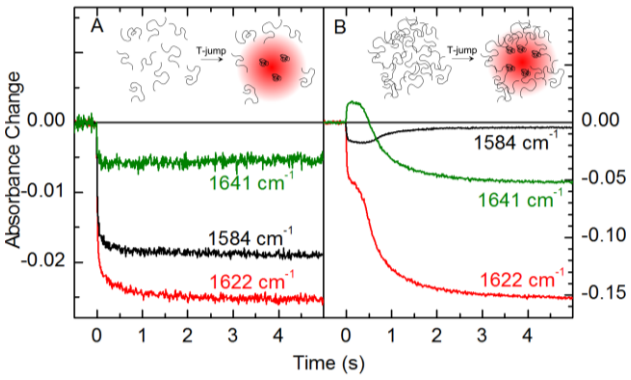

Fig 3. Absorbance changes on the time scale 10 ms to 5 s after a T-jump from 32°C to 40°C at different concentrations of pNIPAm: (A) 10 mg/ml. (B) 45 mg/ml.

The dynamics of the coil-globule transition of pNIPAm after a T-jump over the LCST is characterized by two phases. The first is very fast (<10 ns), and its spectral signature (not shown) corresponds to that expected from the extrapolation of the sub-LCST temperature dependence of the FTIR spectra to temperatures above the LCST. We conclude that even after a T-jump over the LCST, the polymer initially undergoes a similar local collapse as upon a temperature increase below the LCST, involving an increase of the number and/or size of collapsed polymer sections. Due to the local nature of this relaxation, it is not surprising that it proceeds on the nanosecond time scale.

At low concentrations, no further structural changes or phase separation occur up to at least 5 s. However, at higher concentration, phase separation leads to the removal of ~15% of the polymer chains from the heated volume on the 100 ms-time scale. The lowest concentration for this effect to occur is 30 mg/ml, corresponding to a mean polymer separation of 57 Å. This compares reasonably well with the radius of gyration of the coil polymer (R_g ~ 15 Å), suggesting the onset of some overlap/entanglement between polymers. We propose that two conditions are required for polymer chains to undergo the phase separation on the 100 ms time scale observed here: (i) entangled polymer chains, so that the collapsing chains can provide a pulling force, and (ii) a temperature gradient to provide a directional preference for the pulling "force" of the collapsing polymers. This is schematically indicated in the insets to Fig. 3.

Conclusions

IR spectroscopy gives detailed insight into the mechanism and dynamics of the pNIPAm coil-globule transition. An increase of temperature results in fast local collapse of the polymer, followed by much slower aggregation and phase separation. Partial phase separation was observed on the 100 ms time scale, but only if the polymer chains are sufficiently entangled.

Acknowledgements

The authors are grateful for the loan of CLF laser loan pool system CWL1 and for support from the EPSRC. Gold nanoparticles were kindly provided by Dr. R. Levy (Liverpool).

References

1. C. de las Heras Alarcón, S. Pennadam and C. Alexander, *Chemical Society Reviews* **34**, 276 (2005).
2. Z. Ahmed, E.A. Gooding, K.V. Pimenov, L. Wang and S.A. Asher, *Journal of Physical Chemistry B* **113**, 4248 (2009).
3. Y. Tsuboi, et al., *Journal of Physical Chemistry B* **112**, 2562 (2008); *Chemical Physics Letters* **468**, 42 (2009).
4. Y. Maeda, T. Higuchi and I. Ikeda, *Langmuir* **16**, 7503 (2000).
5. H. Kojima and F Tanaka, *Macromolecules* **43**, 5103 (2010).